JOURNAL OF GEOPHYSICAL RESEARCH, VOL. 101, NO. D6, PAGES 10,091–10,127, APRIL 30, 1996

Validation of UARS Microwave Limb Sounder ClO Measurements

J.W. Waters, W.G. Read, L. Froidevaux, T.A. Lungu, V.S. Perun, R.A. Stachnik, R.F. Jarnot, R.E. Cofield, E.F. Fishbein, D.A. Flower, J.R. Burke, J.C. Hardy, L.L. Nakamura, B.P. Ridenoure, Z. Shippony, and R.P. Thurstans

Jet Propulsion Laboratory, California Institute of Technology, Pasadena

L.M. Avallone and D.W. Toohey

Earth System Science Department, University of California at Irvine

R.L. deZafra and D.T. Shindell

Physics Department, State University of New York at Stony Brook

Abstract. Validation of stratospheric ClO measurements by the Microwave Limb Sounder (MLS) on the Upper Atmosphere Research Satellite (UARS) is described. Credibility of the measurements is established by (1) the consistency of the measured ClO spectral emission line with the retrieved ClO profiles and (2) comparisons of ClO from MLS with that from correlative measurements by balloon-based, ground-based, and aircraft-based instruments. Values of "noise" (random), "scaling" (multiplicative), and "bias" (additive) uncertainties are determined for the Version 3 data, the first version publicly released, and known artifacts in these data are identified. Comparisons with correlative measurements indicate agreement to within the combined uncertainties expected for MLS and the other measurements being compared. It is concluded that MLS Version 3 ClO data, with proper consideration of the uncertainties and "quality" parameters produced with these data, can be used for scientific analyses at retrieval surfaces between 46 and 1 hPa (approximately 20–50 km in height). Future work is planned to correct known problems in the data and improve their quality.

1. Introduction

The Microwave Limb Sounder on the Upper Atmosphere Research Satellite is performing the first global measurements of stratospheric chlorine monoxide (ClO), the predominant form of reactive chlorine which destroys stratospheric ozone (O_3). Knowing the amount and global distribution of stratospheric ClO is important since the rate of O_3 destruction by chlorine chemistry can be estimated from the abundance of ClO, and the primary source of stratospheric chlorine is industrial chlorofluorocarbons (CFCs) [*Molina and Rowland*, 1974]. Chlorine destruction of O_3 in the upper stratosphere is proportional to [ClO], the ClO number density. Large springtime loss of Antarctic ozone [*Farman et al.*, 1985] is triggered at low temperatures by heterogeneous chemistry activation of stratospheric chlorine and caused, primarily, by a process proportional to $[ClO]^2$ [e.g., *Solomon*, 1990] where reaction of ClO with itself [*Molina and Molina*, 1987] limits the overall rate.

Techniques which have been developed to measure stratospheric ClO include in situ and remote methods. The in situ technique observes 1189 Å fluorescence from Cl atoms which have been converted from ClO by reaction with NO in a fast flow reactor cell. It has been deployed on parachutes released from balloon [*Anderson et al.*, 1977], reel-down from balloon [*Brune et al.*, 1985], piloted aircraft [*Brune et al.*, 1988], and recently developed for remotely-piloted aircraft [*Toohey et al.*, 1993a]. Remote techniques include heterodyne measurements of millimeter, submillimeter, and infrared spectral lines as well as interferometric observations of submillimeter lines. The millimeter-wavelength heterodyne technique used on UARS MLS has been used previously from aircraft [*Waters et al.*, 1979], ground [e.g., *Parrish et al.*, 1981], and balloon [e.g., *Waters et al.*, 1981]. Submillimeter heterodyne techniques have been used from

Paper number 95JD03351.
0148-0227/96/95JD-03351$05.00

balloon [*Stachnik et al.*, 1992] and aircraft [*Crewell et al.*, 1994], and submillimeter interferometric techniques from balloon [*Carli et al.*, 1988]. The millimeter and submillimeter techniques measure atmospheric thermal emission. Infrared heterodyne measurements were of atmospheric absorption of solar radiation and were conducted from balloon [*Menzies*; 1979, 1983].

This paper describes validation of the UARS MLS ClO measurements. Here "validation" is defined as establishing the credibility of the measurements and their estimated uncertainty (both accuracy and precision). It involves (1) quantifying contributions to the overall uncertainty from various sources (such as instrument noise, calibration and pointing, approximations made in the data processing algorithms, spectroscopic data base, etc.) to the overall uncertainty and (2) comparing the results from MLS with other measurements and "known" behavior of stratospheric ClO to determine whether there is agreement to within the expected uncertainties. *Grose and Gille* [1995] document earlier MLS ClO validation exercises conducted as part of UARS data validation workshops. Companion papers describe calibration of the MLS instrument [*Jarnot et al.*, this issue] and validation of MLS temperature/pressure [*Fishbein et al.*, this issue], H_2O [*Lahoz et al.*, this issue], and O_3 [*Froidevaux et al.*, this issue]. *Froidevaux et al.* [this issue] also give details of the algorithms used for retrieving geophysical parameters from the radiances measured by MLS. The retrievals use a "forward model" which calculates the MLS radiances for a given atmospheric state; this forward model will be described in a future publication (*W.G. Read et al.*, manuscript in preparation, 1996).

The data discussed here are, mainly, the UARS Central Data Handling Facility (CDHF) Version 3 MLS data, the first version publicly released. Results already published which include these data are *Bell et al.* [1994], *Crewell et al.* [1995], *Dessler et al.* [1995], *Douglass et al.* [1993, 1995], *Eckman et al.* [1995], *Elson and Froidevaux* [1993], *Fahey et al.* [1995], *Geller et al.* [1993], *Jones et al.* [1995], *Manney et al.* [1994, 1995a], *Ricaud et al.* [1995], *Santee et al.* [1995], *Schoeberl et al.* [1993] and *Waters et al.* [1993a, b, 1995]. MLS data are available electronically from the Earth Observing System Distributed Active Archive Center at the NASA Goddard Space Flight Center. The "Standard Formatted Data Units (SFDU)" documentation made available with these data describes the format and content of the data files. Names used in the SFDU document are indicated by typewriter font (e.g., `MMAF_STAT`) in this paper.

2. Measurement Description

UARS MLS measurements are obtained from observations of millimeter-wavelength thermal emission as the instrument field of view (FOV) is scanned vertically through the atmospheric limb in a plane perpendicular to the UARS velocity. References which describe the general technique of microwave remote sensing include *Staelin* [1969], *Njoku* [1982], *Ulaby et al.* [1981, 1986], and *Janssen* [1993]. A general description of microwave limb sounding and its features is given by *Waters* [1989, 1993], and the UARS MLS instrument is described by *Barath et al.* [1993].

ClO is measured from the spectral line for the $J = \frac{11}{2} \rightarrow \frac{9}{2}$ rotational transition (J is the quantum number for total angular momentum) of the ^{35}ClO isotope in the ground vibrational ($v = 0$) and electronic ($^2\Pi_{3/2}$) states. Stratospheric emission from this transition is centered near 204,352-MHz frequency (1.47 mm wavelength) and because of nuclear quadrupole effects is split into eight hyperfine components. The hyperfine components are spread over a range of ~25 MHz, and frequencies of all have been measured with ~0.02-MHz accuracy [*Pickett et al.*, 1981]. The ^{35}ClO dipole moment for the $v = 0$, $^2\Pi_{3/2}$ state has been measured to better than 0.1% accuracy [*Yaron et al.*, 1988]. The linewidth parameter for pressure broadening of these transitions by both N_2 and O_2 has been measured with ~3% accuracy as a function of temperature between 200 and 300 K [*Pickett et al.*, 1981; *Oh and Cohen*, 1994].

The top panel of Figure 1 shows atmospheric emission over the spectral region covered by the MLS 205-GHz radiometer which measures ClO. The bottom panels show an expanded region of the spectrum covered by the 205-GHz radiometer in MLS spectral bands B2 and B3 which are used for ClO. It indicates individual filter positions in the two bands and includes contributions from both sidebands of the double-sideband radiometer. B3 was originally included in MLS to measure H_2O_2, when H_2O_2 was predicted to be a major odd-hydrogen reservoir in the middle stratosphere with abundances >10 parts per billion by volume (ppbv) [e.g., *Wofsy*, 1978]. Refinements to parameters used for the theoretical predictions, and measurements [e.g., *Chance et al.*, 1991], now indicate only ~0.1 ppbv H_2O_2 in the stratosphere. The UARS MLS design was "frozen" before discovery of severe ozone loss in the lower stratosphere over Antarctica and when the major concerns were chlorine depletion of ozone in the upper stratosphere. Consequently, the instrument is principally designed for measurements in the middle and upper stratosphere. Lower stratospheric measurements are more difficult with this design than middle to upper stratospheric measurements because the MLS filter banks do not cover as wide a spectral region around the broad spectral lines in the lower stratosphere as would be desired. The additional spectral coverage provided by B3, however, improves MLS measurements of ClO in the lower stratosphere. The double-sideband system noise temperature for bands B2/B3 is 990 K [*Barath et al.*, 1993] and the relative responses from the two sidebands, which are measured as part of instrument calibration and accounted for in data processing, are the same to better than 0.8 dB [*Jarnot et al.*, this issue]. The 1σ noise on individual 1.8 s double-sideband radiance measurements is 0.07 K

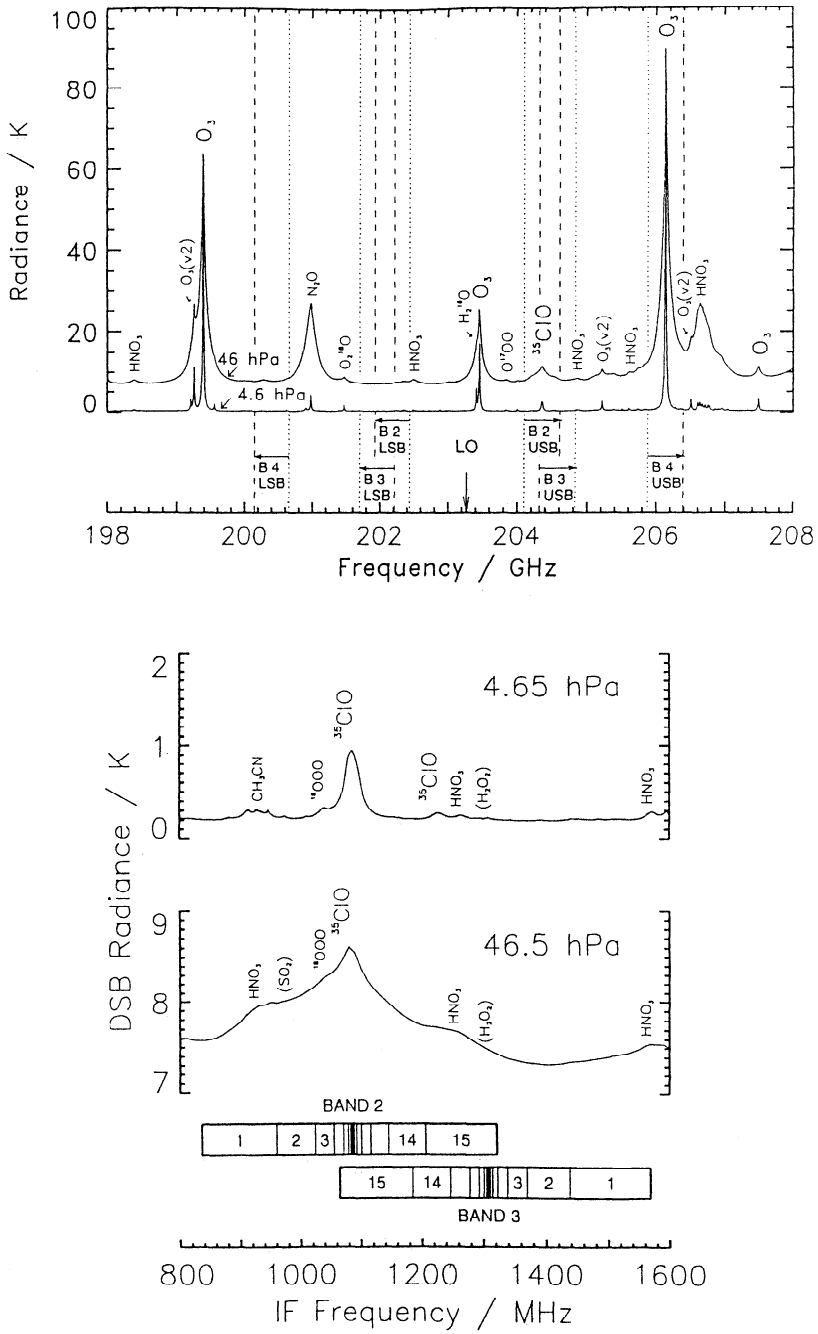

Figure 1. Calculated atmospheric limb radiance for the spectral region containing the 204 GHz ClO line measured by the UARS Microwave Limb Sounder (MLS). The top panel shows the spectrum over the 198 to 208 GHz region and indicates locations of the 205 GHz radiometer local oscillator (LO) and upper (USB) and lower (LSB) sidebands for MLS bands B2, B3 and B4. The bottom panel shows a more detailed view of the region covered by bands B2 and B3 used for ClO, and is a "double sideband" (DSB) calculation (the averaged contributions from the LSB and USB folded about the LO frequency). Locations of the 15 filters in B2 and B3 are indicated in the bottom panel. The "IF frequency" axis on the bottom panel gives the frequency after the first heterodyne conversion in the 205 GHz radiometer; filter channels in B3 increase in the opposite direction than in B2 because of different second-heterodyne conversions in these two bands [*Barath et al.*, 1993]. The vertical scale is the equivalent brightness temperature of the radiance. The calculated spectra are for observation paths through the limb with tangent pressures of 4.6 hPa (upper stratosphere) and 46 hPa (lower stratosphere). The ClO profile used for these calculations was double-peaked to represent lower-stratospheric ClO enhanced by heterogeneous chemistry, and upper-stratospheric ClO due to pure gas-phase chemistry; peak values of 1 part per billion by volume (ppbv) were assumed for both the lower and the upper stratospheric ClO.

for the wide 128-MHz filters at the end of bands and 0.6 K for the narrow 2-MHz filters at band center, and it has been demonstrated that the noise in averages decreases inversely as the square root of the number of measurements averaged, down to at least ~0.005 K for the broadband channels (these values are one-half those in Table 9 and Figure 6 of *Barath et al.* [1993] which are for equivalent single-sideband noise).

The calculated spectra in Figure 1 show signals expected for both upper-stratospheric and enhanced lower-stratospheric ClO. The calculation uses spectroscopic data from the Jet Propulsion Laboratory (JPL) catalog [*Poynter and Pickett*, 1985; *Pickett et al.*, 1992] and includes spectral lines of all molecules (and states) which are thought to be significant [*Waters* 1992, 1993]. ClO is the strongest contributor to daytime stratospheric emission in MLS bands B2 and B3, but there are minor contributions from weak lines of HNO_3, ^{18}OOO, SO_2, and H_2O_2 within these bands. There are also contributions at low altitudes from the wings of H_2O and N_2O lines, and from emission caused by collision-induced absorption among nitrogen and oxygen molecules. MLS measurements of the SO_2 line have been used to obtain vertical profiles of enhanced SO_2 injected into the stratosphere by the Pinatubo volcano [*Read et al.*, 1993]. Lower-stratospheric HNO_3 can also be retrieved [see *Santee et al.*, 1995] from its signature in band B4 used for the 205-GHz ozone measurement, but this was not done in Version 3 processing. Measurements in B2 have also been used to obtain upper-tropospheric H_2O [*Read et al.*, 1995], which is important for climate change research.

Thermal emission from the ClO line is only a weak function of atmospheric temperature. This is because (1) the Planck function at millimeter wavelengths is a weak (linear) increasing function of temperature and (2) the energies of the ClO states involved in the transition (~14 cm^{-1}) are much less than kT, where k is Boltzmann's constant. The state energies being less than kT means that the number of molecules in that state decreases with increasing temperature; this is a larger effect than the temperature-dependence of the Planck function. A +5 K change in atmospheric temperature at 200 K, for example, produces ~−3% change in 204-GHz ClO emission. Atmospheric pressure at the tangent point of the observation path is retrieved from simultaneous observations of 63-GHz thermal emission by molecular oxygen, and this provides the vertical coordinate on which ClO profiles are retrieved.

It can be shown [*Waters*, 1993] that the relative contribution (per unit amount of the emitting species) to the measured limb emission, for optically-thin situations such as the ClO line, has a Gaussian distribution along the observation path (with center at the tangent point, and width approximately equal to the geometric mean of the scale height of atmospheric pressure and the diameter of the Earth). This sets the horizontal resolution along the line of sight (perpendicular to the UARS velocity) to ~400 km. MLS under normal operations performs a complete limb scan with radiometric calibrations every 65.536 s, the MLS Major Frame (MMAF) period. The limb scan covers tangent heights of ~0 to ~90 km, and consists of discrete steps. The scan step spacing used for normal operations [see *Jarnot et al.*, this issue] varies between ~1 km in the lower stratosphere to ~5 km in the mesosphere. A single MLS measurement period is referred to as an MLS Minor Frame (MMIF), which is of 2.048-s duration (1/32 of an MMAF). Atmospheric spectra are measured within an MMIF, during 1.8-s dwells of the FOV between steps. The UARS orbital motion during the time of a limb scan smears the measurement over ~400 km in a direction perpendicular to the MLS line of sight. The horizontal resolution of the ClO measurement is thus ~ 400 × 400 km. The FOV vertical extent (full width at half maximum) at the tangent point for the ClO measurements is 3 km, the approximate inherent vertical resolution of the measurements. As discussed below, the Version 3 data are produced on a vertical grid with points spaced each factor of $10^{1/3} = 2.15$ change in atmosphere pressure, giving a vertical resolution of ~5 km.

The latitudinal coverage of measurements is from 34° on one side of the equator to 80° on the other side. UARS performs a yaw maneuver at ~36-day intervals (a "UARS month"), when MLS high-latitude coverage switches between north and south. The UARS orbit plane precesses slowly with respect to the Earth-Sun line within each UARS month, and local solar times of MLS measurements at a given latitude (on either the "day" or "night" side of the orbit) vary by only 20 min during a 24-hour period. The orbit precession causes the measurements to sweep through essentially all local solar times during the course of a UARS month, becoming 20 min earlier each day at a given latitude.

3. Data Processing for Version 3 ClO

MLS data processing produces individual files containing measurements made over a 24-hour period, from 0 to 24 hours UT on each day. There are two major steps to the processing. The first converts raw "counts" from the instrument telemetry into calibrated radiances and other engineering diagnostics, and produces a "Level 1" file. *Jarnot et al.* [this issue] describe the MLS Level 1 processing and instrument calibration. The second processing step converts calibrated radiances from the Level 1 files into geophysical data, producing a "Level 2" file (geophysical parameters on a vertical grid chosen by the instrument team). Radiances used in the retrievals are those measured on each 2 s MMIF; there is no averaging of the radiances before the retrievals. The Level 2 processing step for MLS also produces "Level 3A" files, which are geophysical parameters on a vertical grid common to all UARS instruments producing atmospheric profiles. There are

two Level 3A files: (1) "Level 3AT" which has profiles equally spaced in time intervals of 65.536 s and (2) "Level 3AL" which has profiles equally spaced in latitude intervals of 4°. Accompanying the Level 3AT and 3AL files are "parameter" files, "Level 3PT" and "Level 3PL" files, which contain various parameters providing diagnostics of the data. "Level 3B" files, which contain data commonly-gridded in the horizontal for all UARS instruments producing Level 3AL files, are produced from the Level 3AL files (*C.A. Reber et al.*, manuscript in preparation, 1996).

A complete MLS limb scan under normal operations is performed for each 65.536 s MMAF and, during Level 2 processing, a ClO profile is retrieved from the radiances measured on each limb scan. Sequential estimation, as first applied to atmospheric remote sensing by *Rodgers* [1976], is used. Values of the MLS "state vector" $\boldsymbol{x}$ and its error covariance matrix $\boldsymbol{S}$ are sequentially estimated from the measured radiances y_i, starting at highest tangent heights and working downward, according to the recursion formulae

$$\widehat{\boldsymbol{x}}_i = \widehat{\boldsymbol{x}}_{i-1} + \frac{\widehat{\boldsymbol{S}}_{i-1}\boldsymbol{K}_i\{y_i - [\overset{\star}{\boldsymbol{y}}^c + \boldsymbol{K}(\widehat{\boldsymbol{x}}_{i-1} - \overset{\star}{\boldsymbol{x}})]_i\}}{\boldsymbol{K}_i^T\widehat{\boldsymbol{S}}_{i-1}\boldsymbol{K}_i + \widehat{\epsilon}_i^2 + \omega_i^2} \quad (1)$$

$$\widehat{\boldsymbol{S}}_i = \widehat{\boldsymbol{S}}_{i-1} - \frac{\widehat{\boldsymbol{S}}_{i-1}\boldsymbol{K}_i\boldsymbol{K}_i^T\widehat{\boldsymbol{S}}_{i-1}}{\boldsymbol{K}_i^T\widehat{\boldsymbol{S}}_{i-1}\boldsymbol{K}_i + \widehat{\epsilon}_i^2 + \omega_i^2} \quad (2)$$

where $i = 1, 2, \ldots, N$ ranges over the set of radiances used from each limb scan, $\widehat{\boldsymbol{x}}_0$ and $\widehat{\boldsymbol{S}}_0$ are given by a priori values, and $\widehat{\boldsymbol{x}}_N$ and $\widehat{\boldsymbol{S}}_N$ are the resulting retrieved values for that limb scan. The retrieval is linearized about $\overset{\star}{\boldsymbol{x}}$, and $\overset{\star}{\boldsymbol{y}}^c$ is a tabulated vector of radiances at "standard" tangent pressures which are calculated from $\overset{\star}{\boldsymbol{x}}$ using the MLS "forward model." $\boldsymbol{K}$ is a tabulated matrix of calculated partial derivatives of $\boldsymbol{y}^c$ with respect to $\boldsymbol{x}$, having elements $K_{\alpha\beta} = \partial y_\alpha^c / \partial x_\beta$ where y_α^c is element α of $\boldsymbol{y}^c$ and x_β is element β of $\boldsymbol{x}$, and are evaluated at $\boldsymbol{x} = \overset{\star}{\boldsymbol{x}}$; superscript T indicates transpose. The subscripts i on $\boldsymbol{K}$ in (1) and (2) indicate a row vector which has been interpolated (linearly in logarithm of tangent pressure) from the rows in $\boldsymbol{K}$ to the retrieved tangent pressure for y_i. The subscript i on the bracketed quantity in the numerator of (1) indicates a value obtained by cubic-spline interpolation of its element values to the retrieved tangent pressure for y_i. The estimated noise variance for the measurement y_i is given by $\widehat{\epsilon}_i^2$, and ω_i^2 accounts for additional uncertainty contributions not covered by the $\boldsymbol{K}_i^T\widehat{\boldsymbol{S}}_{i-1}\boldsymbol{K}_i$ and $\widehat{\epsilon}_i^2$ terms in (1) and (2). See *Froidevaux et al.* [this issue] for more details on the MLS Version 3 retrieval algorithms.

Vertical variation of the ClO profile, for MLS Version 3 Level 2 data, is represented as piecewise-linear in mixing ratio versus logarithm of atmospheric pressure with breakpoints at $10^{(6-n)/3}$ hPa, where n is an integer from 0 to 7 covering the 100 to 0.46 hPa range of pressures for which meaningful ClO retrievals are performed. Retrieved values at the breakpoints of this representation (100, 46, 22, 10, 4.6, 2.2, 1.0 and 0.46 hPa) constitute the ClO subset of the elements of $\widehat{\boldsymbol{x}}$; additional elements of $\widehat{\boldsymbol{x}}$ include other parameters (H_2O, O_3, temperature, tangent pressure, etc.) retrieved from the MLS data, and a description of the complete MLS state vector is given by *Froidevaux et al.* [this issue]. The retrieved profile should be interpreted as that which "best fits" the measured radiances, within the limitations of the retrieval algorithms and representation bases, and the values retrieved for the breakpoints of the piecewise-linear representation should not be interpreted as "point" measurements at that location.

Band B2 and B3 radiances measured between retrieved tangent pressures of 0.46 and 100 hPa are used for the ClO retrievals. The calibrated MLS radiances are produced from raw instrument data by Level 1 algorithms [*Jarnot et al.*, this issue] which also produce estimates of the measurement noise $\sqrt{\widehat{\epsilon}_i^2}$ for each measured radiance y_i. A "spectral baseline," consisting of a constant offset and a linear variation with frequency, is fitted to the combined radiances measured in bands B2 and B3 on each MMIF; this prevents radiance "offsets" and slopes, which are not completely accounted for by the forward model, from affecting the retrievals. The retrieved spectral baseline parameters are part of the estimated state vector $\widehat{\boldsymbol{x}}$, and their uncertainties are included in the overall uncertainty estimated for ClO. No radiances are used from observations for which the inferred tangent pressure is greater than 100 hPa, in order to eliminate tropospheric effects which could have spectral curvature and might not be adequately accounted for in the forward model. The algorithms also use no radiances when the inferred optical depth for the observation path is greater than unity (although this should not happen for bands B2 and B3 at tangent heights above 100 hPa), to avoid situations where there might be a large non-linear relation between radiances and ClO mixing ratio.

Values of the partial derivatives $\boldsymbol{K}$ and the calculated radiances $\overset{\star}{\boldsymbol{y}}^c$ are produced, for each UARS month and selected latitude bins, from the MLS forward model, as described by *W.G. Read et al.* (manuscript in preparation, 1996). Elements of $\boldsymbol{K}$ and $\overset{\star}{\boldsymbol{y}}^c$ correspond to each of the standard UARS Level 3A pressure surfaces (described below). The forward model accounts for the instrumental frequency and angular smearing of the radiances (including refraction), using measured values for the FOV and filter responses obtained during instrument calibration. It accounts for the hyperfine splitting in the 204-GHz ClO line, and the temperature-dependent populations of the rotational states involved, including the fraction of ClO in the $^2\Pi_{1/2}$ spin state (11% at 220 K); excited vibrational states have negli-

gible population (about 0.4% at 220 K; see discussion by *Waters et al.* [1979]). Numerical errors resulting from software implementation of the forward model are estimated to contribute less than 0.02 K accumulated uncertainty in the calculated spectral variation of the signals measured by MLS bands B2 and B3 at tangent heights above 100 hPa. After the Version 3 data were produced, however, it was discovered that an "old" ClO line strength file had been inadvertently used in calculating the $\boldsymbol{K}$ and $\overset{\star}{\boldsymbol{y}}^{c}$; this causes the Version 3 ClO values to be too large by 8%, and all MLS Version 3 ClO values need to be multiplied by 0.92 to correct for this error.

HNO_3 and, to a lesser extent, N_2O have a small effect on the ClO signal and are accounted for in the Version 3 algorithms by assuming (latitudinal and seasonal dependent) climatological values [*Gille et al.*, 1989; *Taylor et al.*, 1989]. The effects of the ozone isotope ^{18}OOO are accounted for by multiplying the retrieved O_3 profile by 4.06×10^{-3}, based on the 2.04×10^{-3} relative abundance of ^{18}O [*Craig*, 1957]; variations in the relative isotopic abundance with altitude [*Mauersberger*, 1987] are not included. The effects of SO_2 on ClO are included, since the Version 3 algorithms simultaneously retrieve SO_2 and ClO. Emission due to collision-induced absorption among N_2 and O_2 molecules is included by an empirical model determined from the MLS radiances (*W. G. Read et al.*, manuscript in preparation, 1996).

A retrieval is done for each limb scan, with the retrieval algorithm having no "memory" of ClO results from any other limb scan. The ClO retrieval is done after retrievals for all other elements of the state vector $\boldsymbol{x}$ have been completed, so that values of $\widehat{\boldsymbol{S}}$ and $\widehat{\boldsymbol{x}}$ at the beginning of the ClO retrieval have been updated for all "non-ClO" elements. This accounts, through appropriate elements of $\boldsymbol{K}$, for effects of other retrieved parameters on the retrieved values of ClO. The a priori used for the "pure ClO" portion of $\widehat{\boldsymbol{S}}$ is diagonal, with values corresponding to 4 ppbv 1σ uncertainty in total ClO (3 ppbv 1σ uncertainty in the ^{35}ClO isotope measured by MLS) for atmospheric pressures between 100 and 0.46 hPa, intentionally very conservative to reduce effects of the a priori on the result. The ClO profile below 100 hPa is also formally "retrieved" as part of the sequential estimation process, but MLS does not provide significant information at these low altitudes and the retrieval is more tightly constrained to the a priori (an a priori uncertainty of 0.7 ppbv is used at 215 hPa and 0.1 ppbv at 464 hPa). The ClO a priori values depend upon latitude, UARS month, whether the measurement was made during day or night, and are from a gas-phase model prediction (provided by D.J. Wuebbles and colleagues) which includes no heterogeneous chemistry enhancement of lower-stratospheric ClO.

The retrieved ^{35}ClO mixing ratios are multiplied by 1.32 to give the total ClO mixing ratio in both ^{35}ClO and ^{37}ClO isotopes. This assumes 75.8% of chlorine is in the ^{35}Cl isotope [*Shields et al.*, 1962].

UARS Level 3A files have values on pressure surfaces of $10^{-m/6}$ hPa where m is an integer, the spacing between Level 3A surfaces being half that of the MLS Version 3 Level 2 surfaces (i.e., there are twice as many Level 3A surfaces as MLS Level 2 surfaces). Averages of the two values on adjacent MLS Level 2 surfaces are put in the Version 3 MLS Level 3A files for the UARS surfaces on which MLS retrievals are not performed. Level 3AL files are produced by interpolating the MLS Level 3AT data to the 3AL latitudes $(0, \pm4^\circ, \pm8^\circ, \ldots)$.

An estimated uncertainty is placed in the MLS Level 2 and Level 3 files for each value retrieved for ClO. This uncertainty is from the appropriate diagonal element of $\widehat{\boldsymbol{S}}$ at the end of each profile retrieval. The estimated uncertainty is made negative if it has not been reduced to less than one half of the a priori uncertainty, to flag situations when the a priori is weighted into the result by more than 25%. Several additional diagnostics are routinely produced during data processing and placed in the Level 2 files. The extent to which the retrieved profile "fits" the measured radiances is described by a χ^2 diagnostic [see *Froidevaux et al.*, this issue]. This diagnostic has a value near unity if radiances calculated from the retrieved parameters (using a linearized "forward model") agree with the measured radiances to within the expected instrument noise. The χ^2 diag-

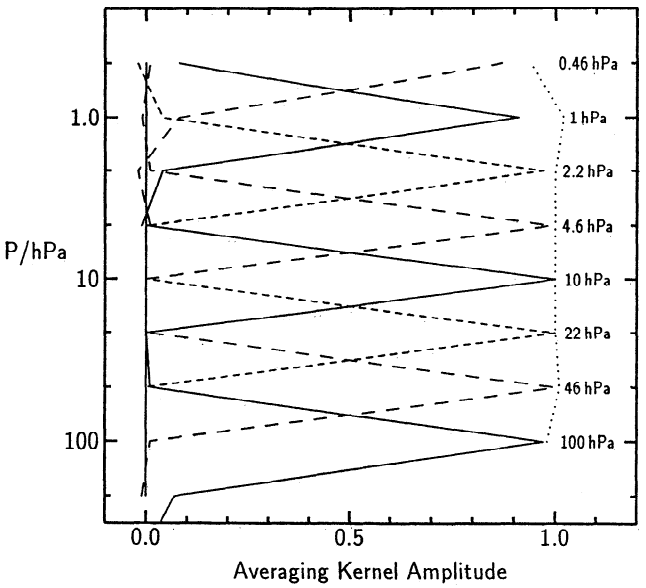

Figure 2. Averaging kernels [see *Rodgers*, 1990; *Marks and Rodgers*, 1993] for MLS Version 3 ClO profile retrievals. The solid and dashed curves are the rows of the averaging kernel matrix and give the vertical resolution in the retrieved profile. The number printed to the right of each peak is the pressure of the retrieval surface associated with that kernel. The dotted line is the sum of the columns of the averaging kernel matrix for that height and gives the relative amount of information which comes from the MLS measurement, as opposed to coming from the a priori.

nostics are produced for each MLS band, and both for radiances (1) measured during each 1.8 s MMIF (χ^2_{mi}) and (2) measured over all tangent pressures down to 46 hPa during the limb scan for each MMAF (χ^2_{ma}). A quality indicator for each ClO retrieval (`QUALITY_CLO`), based on χ^2_{ma} for band B2, is placed in the MLS L3PT and L3PL files. Only data having `QUALITY_CLO=4`, corresponding to $\chi^2_{ma} \leq 2.0$, should be used for scientific analyses. Another important parameter placed in the MLS 3PT and 3PL files is `MMAF_STAT`, which gives the overall status of MLS data for that `MMAF`. Only data having `MMAF_STAT=G` (good) should be used for scientific analyses.

The retrieved ClO profile points have not been constrained to positive values and, since the signal-to-noise ratio for individual ClO measurements is generally less than unity, negative values often occur. This is required for maintaining a linear relation between the retrieved profile points and the measured radiances, to allow averaging of individual retrieved profiles for reducing measurement noise. If the retrieved ClO profiles were not allowed to go negative (which would have been the case, for example, if logarithm of mixing ratio had been retrieved) and the actual amount of atmospheric ClO were zero, for example, then averaging the retrieved profiles would necessarily produce an incorrect non-zero result since instrument noise would only be allowed to produce non-negative values. Tests have shown that the same result for ClO is obtained by averaging the individual retrieved profiles as by performing a retrieval on averaged radiances. Much less effort is required in averaging the available individual profiles than in averaging the radiances and then doing additional retrievals; this is a major benefit of appropriately allowing negative values in individual retrievals.

Averaging kernels [*Rodgers*, 1990], which describe the vertical resolution of retrievals and their dependence upon the a priori, are shown in Figure 2 for the MLS Version 3 ClO. Summations over the averaging kernel columns have value near unity, which indicate that the MLS ClO retrievals between 100 and 0.46 hPa are essentially independent of the a priori; their width indicates that the vertical resolution is approximately equal to that of the retrieval grid spacing (factor of $10^{1/3}$ change in atmospheric pressure, or ~5 km). Much of the smoothing present in the Version 3 data is due to the coarseness of the retrieval grid, and the averaging kernels shown here were calculated using the same vertical representation basis as the retrievals. The MLS averaging kernels are much narrower (especially in the lower stratosphere) and have peak values much closer to unity than those given by *Aellig et al.* [1993] for ClO measured by the same technique. The difference is due, mainly, to differences in the assumed a priori uncertainties. *Aellig et al.* [1993] assume an a priori ClO uncertainty ranging from less than 0.1 ppbv below 30 km and above 56 km to 0.7ppbv at 40 km; this causes the a priori to have a much larger effect (which reduces the peak values of the averaging kernels and broadens them) in their retrievals than in ours where an a priori uncertainty of 4 ppbv is used at all altitudes between 100 and 0.46 hPa.

4. Radiances and Closure

An important aspect of validating MLS ClO is examination of the measured radiances and the extent to which these are "fit" by radiances calculated from the retrieved profiles. Thirty spectral channels in MLS bands B2 and B3 are used for retrieving ClO from MLS. These channels resolve the ClO emission feature at all altitudes throughout the stratosphere, allowing clear identification of the ClO signal. Approximately 500 spectral points in each limb scan are used to retrieve the 8 ClO profile values, the 4 SO_2 profile values, and approximately 36 "spectral baseline" values (offset and slope for each measured spectrum used in the ClO retrievals). Since there are many more measurements than retrieved parameters, examination of the residuals is a meaningful exercise.

Figure 3 shows averages of measured lower-stratospheric radiances and residuals for conditions of enhanced lower-stratospheric ClO in the Antarctic vortex in mid-August, where largest ClO abundances are measured by MLS [*Waters et al.* 1993a]. Also shown are the radiances calculated from the Version 3 retrieved profiles and the residuals (measured minus calculated radiances). The radiance is given as double-sideband "brightness temperature," a quantity which, when multiplied by Boltzmann's constant, gives the average spectral power density (Watts/Hertz) received through each filter. It should be noted that the full Planck function, and not the Rayleigh-Jeans approximation which is sometimes used for microwave calculations, is used for the MLS calculation. The "double-sideband" units are due to the fact that the blackbody radiometric calibration used for MLS gives signals in both sidebands of the double-sideband radiometers, whereas the ClO spectral line appears in only one of the sidebands; the "single-sideband" ClO signals would be approximately twice as strong as the double-sideband signals shown here. The good fit between measurement and calculation is evident in Figure 3, and there is closure to within ~0.2 K brightness temperature.

The narrower spectral feature from upper stratospheric ClO is shown in Figure 4. Also shown are averages of the radiances calculated from the retrieved ClO, and the residuals. The closure is within 0.05 K brightness temperature. The extent to which the lack of closure introduces errors in the retrievals is discussed in section 5 of this paper.

Figure 5 shows averages of spectra measured at tangent height above ~65 km, where the ClO signal (if present at all) would be confined to the narrow center channels, and illustrates residual artifacts in the measured radiances. These artifacts have a spectral vari-

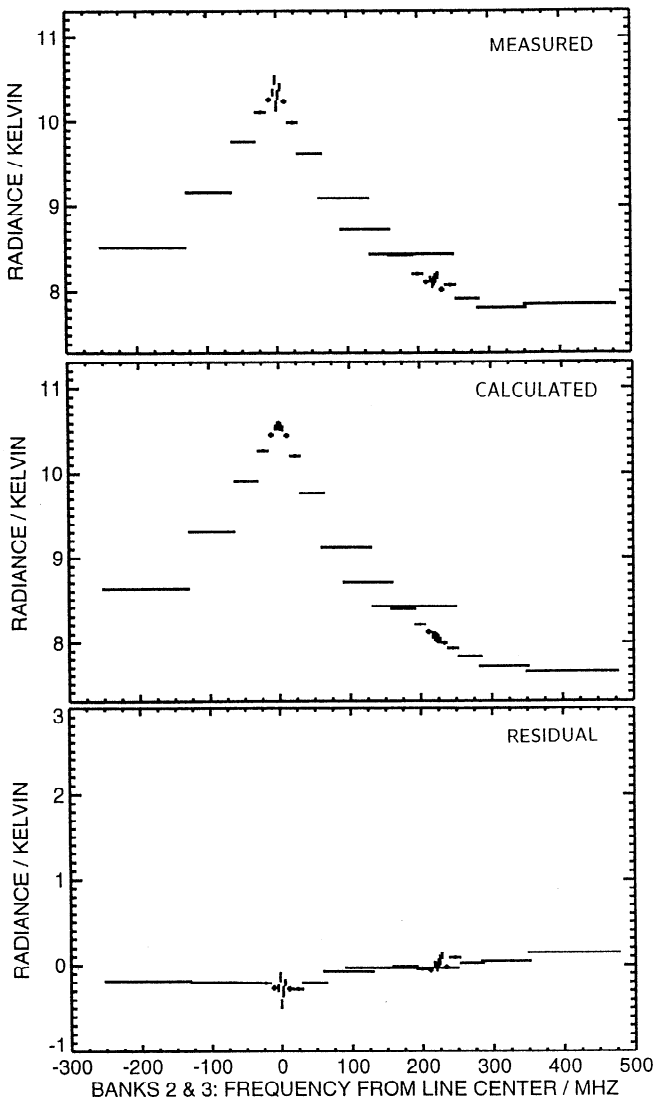

Figure 3. Lower-stratospheric ClO spectra from the Antarctic vortex. Top panel is the average of measurements made with the MLS field-of-view (FOV) between 22- and 100-hPa tangent pressures (~13–22 km) on 16 separate limb scans occurring during daylight at local solar zenith angles (SZA) less than 85° on 16 August 1992. The limb scans were selected from the region where largest ClO abundances are retrieved, and only data having MMAF_STAT=G and QUALITY_CLO=4 were included. Middle panel is the average of spectra for the same tangent heights calculated from the individual retrievals. Bottom panel shows the average of the residuals (measured minus calculated). Horizontal bars indicate the different filter channels, and the width of each bar gives the width of that filter. The vertical bars give the expected noise of the average.

ation of ~0.05 K brightness temperature, which yield artifacts in retrieved ClO abundances of ~0.05 ppbv. They appear sufficiently stable that day-night differences are expected to reduce the instrumental artifacts to approximately 0.01 K brightness temperature, corresponding to ClO abundances of approximately 0.01 ppbv. Improved Level 1 data processing algorithms have been developed, and will be used in future processings of MLS data, which reduce these artifacts to ~0.01 K without requiring day-night differences.

Plate 1 shows, for bands B2 and B3 and the first 3 years of MLS operation, daily zonal averages of the diagnostic χ^2_{ma} which measures goodness-of-fit to the measured radiances of those calculated from the retrieved

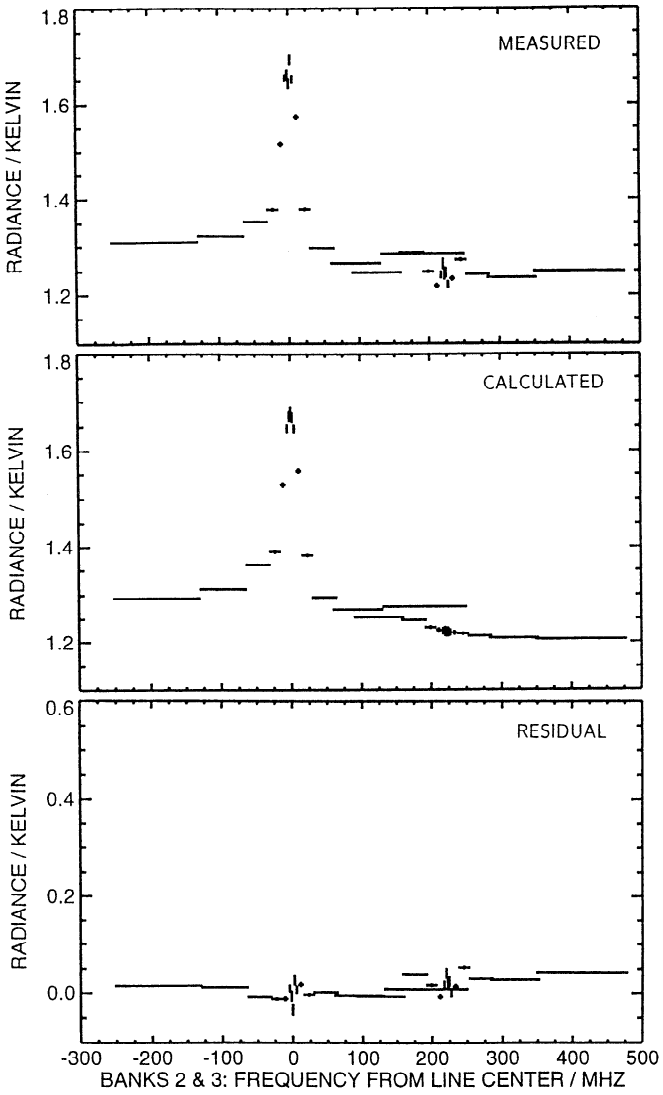

Figure 4. Middle-upper stratospheric ClO spectra. Top panel is the average of measurements made with the MLS FOV between 2.2- and 10-hPa tangent pressures (~31–42 km) on 548 separate limb scans occurring during daylight at local SZA<80° on 11 July 1993. The average encompasses the complete 34° S to 80° N range of latitudes sampled by MLS on this day. Only data having MMAF_STAT=G and QUALITY_CLO=4 have been included. Middle panel is the average of spectra for the same tangent heights calculated from the individual retrievals. Bottom panel shows the average of the residuals (measured minus calculated). Horizontal bars indicate the different filter channels, and the width of each bar gives the width of that filter. The vertical bars give the expected noise of the average. Note that the vertical scale has been greatly expanded from that in Figure 3.

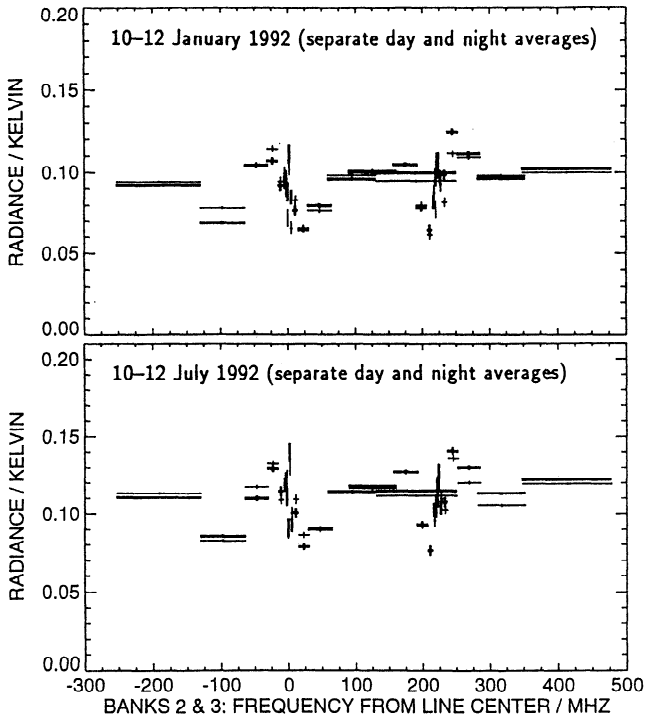

Figure 5. MLS "space radiances" averaged separately for two 3-day periods. Only radiances having inferred tangent pressure less than 0.1 hPa (heights above about 65 km) are included in the average. The top panel is for 10–12 January 1992 (north-looking, covering latitudes 34° S to 80° N), and the bottom panel is for 10–12 July 1992 (south-looking, covering latitudes 80° S to 34° N). The two spectra in each panel are the separate averages for "day" (thick pluses; SZA<90°) and "night" (thin pluses; SZA>90°). The spectral pattern for these high altitudes is due to residual artifacts in the Version 3 processing. Averages are of approximately 9000 individual spectra, each measured with an instrument integration time of 2 s, and only data having `MMAF_STAT=G` and `QUALITY_CLO=4` have been included.

profiles. Values are generally in the 1.25–1.75 range, indicating reasonable fits but with room for improvement. The gaps in June 1992 are due to MLS being off during a UARS solar array drive problem, and B3 was off while B2 remained on during portions of late June and early July 1992. The large χ^2_{ma} values at northern midlatitudes in October and November 1992 are due to development of excess noise induced by the MLS switching mirror movement at times when the UARS power supply voltage was at its lowest (near sunrise on the spacecraft). After investigation of this induced noise the MLS instrument was determined to be sufficiently stable that calibration is not needed on each limb scan; its operation was then adapted to sense low-voltage situations, and the switching mirror was not moved in those situations. This adaptation was implemented between 18 November 1992 and 2 June 1993, after which performance (as measured by the χ^2_{ma} diagnostic) improved. The occurrences of occasional large χ^2_{ma} values after June 1993 are when there were abnormal operations. The 1-day gaps in April-May and July 1994 are when MLS was operated every other day during "summer" UARS months, to conserve lifetime of the antenna scan actuator which developed problems starting in late December 1993.

5. Uncertainties in Version 3 ClO

Uncertainties in the MLS ClO data, for use in scientific analyses, are conveniently grouped into three categories: (1) noise, a random contribution which can be reduced by averaging (this is the "precision" of the measurement); (2) scaling, a "multiplicative" uncertainty which gives the "percentage" uncertainty in the measurements; and (3) bias, an "additive" uncertainty which can sometimes be reduced by taking appropriate differences.

"Noise" Uncertainties

The estimated random noise uncertainty ($\pm 1\sigma$) associated with each retrieved ClO profile point is obtained from the appropriate diagonal element of the estimated covariance matrix computed by the retrieval algorithms and is stored along with the retrieved values in the MLS data files. It includes the effects of noise uncertainties associated with temperature, pointing (tangent pressure of the observation path), water vapor, fitted spectral baseline, and other parameters which are part of the overall state vector for the MLS retrievals. As stated earlier, the estimated uncertainty resulting from the retrieval is multiplied by −1 if it has not been reduced to less than one-half the assumed a priori uncertainty; this negative value flags situations where the a prior is weighted into the result by more than 25%.

Figure 6 compares the 1σ noise uncertainties predicted by the retrieval algorithms with the observed standard deviation in retrieved ClO profiles under conditions when instrument noise is expected to dominate. Each panel shows results for a full UARS month (summer in each hemisphere) of retrievals from measurements made at night with local solar times between midnight and 0600 (no retrievals were included for which the solar zenith angle at the time and place of measurements was less than 95°). More than 10,000 independent retrievals were included for the results shown in each panel. The standard deviation of the measurements agrees closely with the predicted 1σ noise, except at the lowest altitude (100 hPa). The primary reason for the 100-hPa ClO estimated noise being larger than the observed variation in retrieved values is that the Version 3 algorithms do not adequately account for correlations in the noise from certain sources. Specifically, the spectrally-constant and spectrally-linear effects on ClO radiances at low altitudes due to H_2O, O_3 and other sources are effectively removed by retrieval of the "spectral baseline," but the Version 3 algorithms assume that these effects on ClO are independent. The result is that

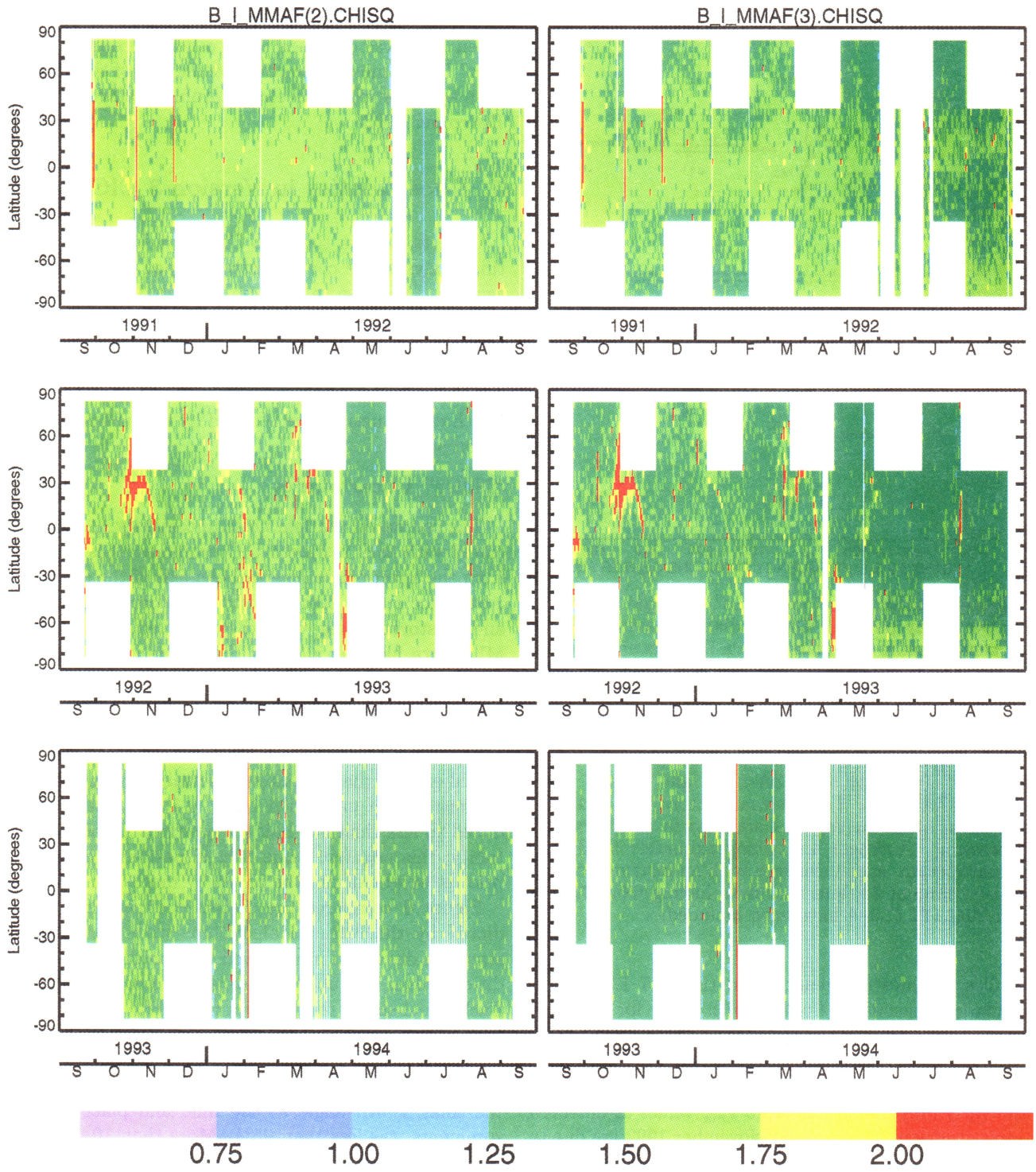

Plate 1. Daily zonally-averaged χ^2_{ma}, the chi-square statistic which measures goodness-of-fit of the retrieved profile to the measured radiances, for MLS ClO retrievals for the first three years of MLS measurements. Values are shown separately for (left) MLS band 2 and (right) band 3. Gaps occur where there were no measurements; the alternating gaps during April–May and July 1994 are when MLS was operated every other day.

the ω_i^2 term in equations (1) and (2) is larger than it should be: the ClO radiances at lowest altitudes are not weighted sufficiently in the retrievals and the ClO error covariance is not adequately reduced. An additional minor part of the 100-hPa uncertainty discrepancy is due to the fact that the predicted uncertainty includes a contribution from the assumed 4 ppbv a priori uncertainty, whereas a constant a priori value (0.0 ppbv at 100 hPa) with no noise is used in the retrievals.

Figure 7 shows the distribution, on each retrieval pressure surface, of values of the nighttime ClO retrievals which were included in Figure 6 (a total of

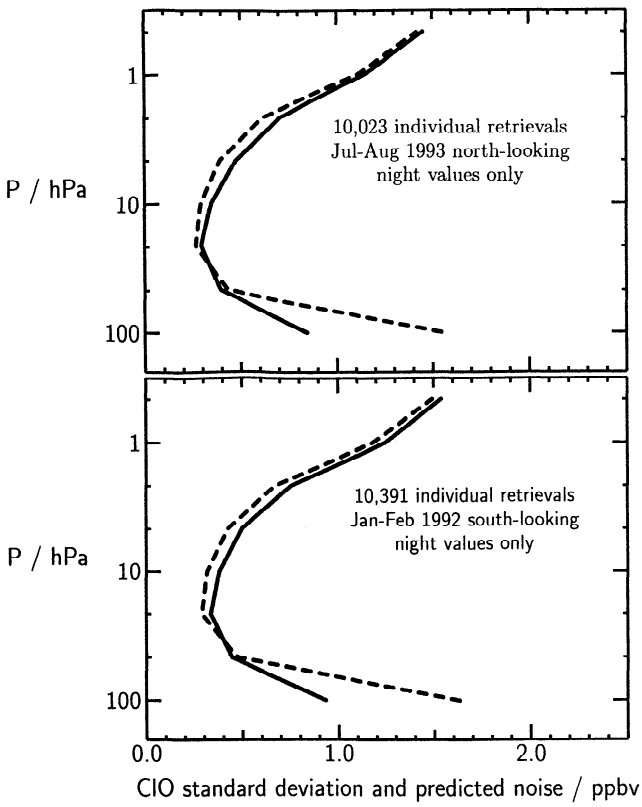

Figure 6. Measured standard deviation (solid) and predicted 1σ noise (dashed) in individual MLS ClO retrievals. The data sample here included only retrievals made in early morning (SZA>95° and local solar times between midnight and 0600) during the 9 July to 8 August 1993 north-looking period (top, covering latitudes 34° S to 80° N) and the 15 January to 14 February 1992 south-looking period (bottom, covering latitudes 80° S to 34° N). This sample covers times when ClO atmospheric variability is expected to contribute minimally, and the observed standard deviation should be dominated by instrument noise. The predicted 1σ noise is the average value for each data ensemble of the values produced by the retrieval algorithms. These results are from Version 3 data which have been multiplied by 0.92, and only records having `MMAF_STAT=G` and `QUALITY_CLO=4` were included (see discussion in text).

more than 20,000 retrievals). The distribution is seen to be Gaussian, as expected for random noise, and supports our understanding of the random noise uncertainties in MLS ClO. *Schoeberl et al.* [1993] also found Gaussian distributions of night and extra-vortical ClO values from MLS which are consistent with those expected from the noise.

"Scaling" Uncertainties

Figure 8 summarizes the estimated contributions to the scaling uncertainties, and the bases for these estimates are described below. As mentioned earlier, an outdated ClO line strength file was inadvertently used in producing the MLS Version 3 data, causing the retrieved ClO values to be 8% too large. The scaling uncertainties described here apply to the Version 3 ClO values after they have been multiplied by 0.92 to correct this error.

ClO is retrieved from optically-thin radiance measurements and there is, to within a good approximation, a linear relationship among the ClO abundances, absorption coefficient, and radiances: the same scaling uncertainties in radiances and absolute values of the ClO absorption coefficient thus apply to the retrieved profiles. An overall instrument calibration uncertainty of 3% is used [*Jarnot et al.*, this issue]. "Calibration uncertainty" is here defined as the combined systematic uncertainty in the calibrated radiances from each instrument channel and that introduced by instrument parameters in calculations of the radiance by the retrieval forward model (which uses the measured instrument spectral and field-of-view response); this includes,

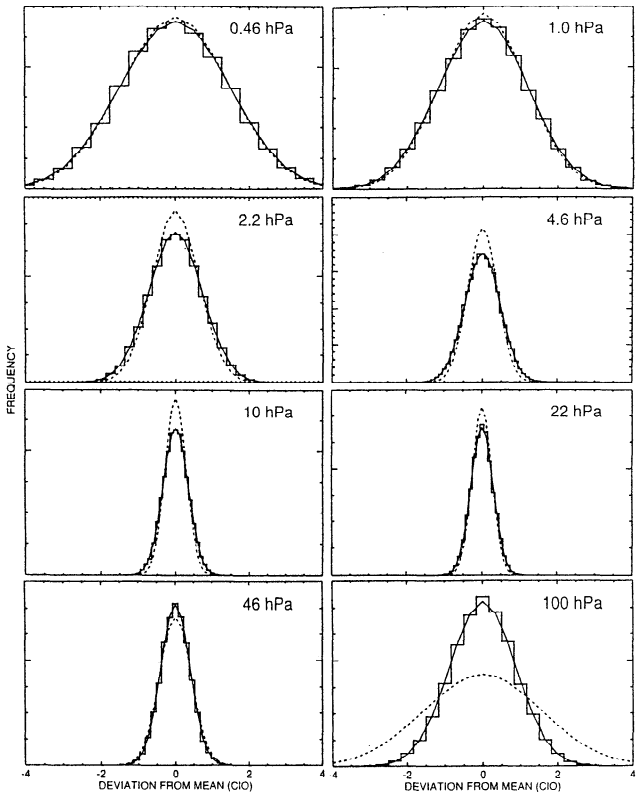

Figure 7. The distribution of nighttime ClO values whose standard deviations are shown as the solid lines in Figure 6. The data ensemble used here includes 20,414 individual profiles when the retrieved distribution is expected to be dominated by instrument noise. The "staircase" histograms in each panel give show the measured distribution of the retrieved values. Only data having `MMAF_STAT=G` and `QUALITY_CLO=4` have been included. The horizontal axis is deviation from the mean (in ppbv) and the vertical axis is the relative frequency of occurrence of values within the 0.25 ppbv increments chosen for the histogram. The smooth curves are Gaussians having approximately the same enclosed area as the histograms. The solid Gaussian has width equal to the measured standard deviation of the data, and the dashed has width equal to the average of the uncertainties predicted by the Version 3 algorithms.

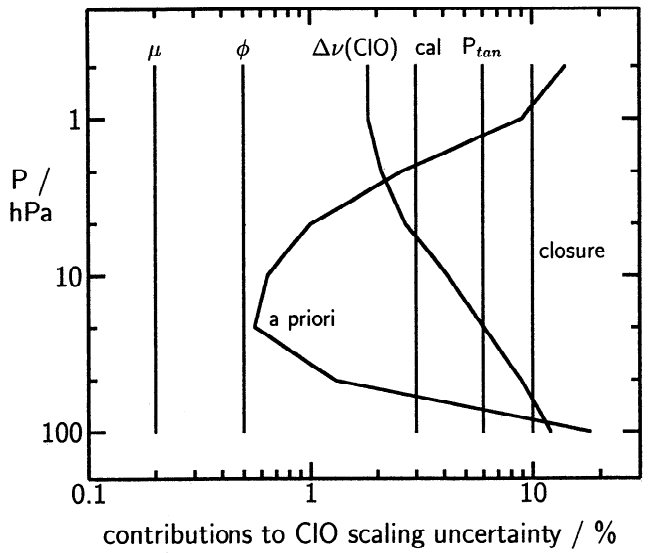

Figure 8. Estimated contributions to "scaling" uncertainties for MLS Version 3 ClO (after the Version 3 values have been multiplied by 0.92 as discussed in the text). The curve labeled μ is due to ClO dipole moment, ϕ to 204 GHz transition matrix element, $\Delta\nu$(ClO) to ClO linewidth, P_{tan} to tangent pressure, "cal" to instrument calibration, "closure" to lack of retrieval closure, and "a priori" is maximum effect of a priori.

for example, uncertainties arising from the relative sideband responses of the radiometers and in alignment of the FOVs of different radiometers. The same radiometer, optics path, and calibration are used for the MLS ClO measurements as for its 205-GHz ozone measurements, so that validation of the ozone measurements [*Froidevaux et al.*, this issue] contributes confidence to calibration of the instrument for ClO measurements. Uncertainties in the absolute value of the absorption coefficient are due to uncertainties in the measured dipole moment of ClO and in the calculated matrix element for the particular transition observed by MLS. The 0.1% uncertainty in the dipole moment [*Yaron et al.*, 1988] introduces an 0.2% error since the square of the dipole moment appears in the expression for the absorption coefficient. The uncertainty in the calculation of the transition matrix element is estimated to be 0.5% (H.M. Pickett, private communication, 1995).

The MLS spectrally-resolved radiance measurements provide information on the ClO spectral line shape and width. After radiance residuals from Version 1 processing indicated a potential problem with the ClO pressure-broadening linewidth parameter used there, an "off-line" retrieval scheme was implemented which allowed retrieval of the ClO linewidth simultaneously with the other parameters normally retrieved. Results gave ~10% smaller value than the N_2 broadening parameter measured by *Pickett et al.* [1981]. The 204-GHz ClO line broadening, by both O_2 and N_2, was then measured over a temperature range of 200–300 K by J.J. Oh and E.A. Cohen in the laboratory at JPL; they found values for N_2 in agreement with those of *Pickett et al.* [1981] but smaller broadening by O_2 and a net air-broadening parameter which was consistent with the value retrieved from MLS. The new laboratory measurements [*Oh and Cohen*, 1994] have an estimated accuracy of ~3% and were used in the production of MLS Version 3 ClO data. The effect of the linewidth parameter uncertainty was determined by propagating it through the retrieval algorithms; we used 6% as a conservative 2σ estimate of the maximum uncertainty on the ClO linewidth, and this gives the "$\Delta\nu$(ClO)" curve shown in Figure 8.

The a priori introduces a "multiplicative" uncertainty into the MLS retrievals, as its effect is proportional to the difference between the true ClO profile and that assumed for the a priori. A worst-case "scaling" uncertainty can be estimated, as follows, by assuming an a priori profile which is identically zero. Neglecting off-diagonal terms in the covariance matrix, the retrieved value $\hat{x}$ is obtained by combining the a priori value x_a and the "pure MLS" value x_m according to $\hat{x} = \hat{\sigma}^2(x_m/\sigma_m^2 + x_a/\sigma_a^2)$, where σ_m is the uncertainty associated with the "pure MLS" measurement, σ_a is the uncertainty assumed for the a priori, and $\hat{\sigma}$ is the resulting overall uncertainty when the "pure MLS" and a priori "measurement" are combined ($\hat{\sigma}^{-2} = \sigma_m^{-2} + \sigma_a^{-2}$). For an a priori of zero ($x_a = 0$) the "pure MLS" measurement is thus seen to be scaled by $\hat{\sigma}^2/\sigma_m^2$. The scaling error is then $1 - \hat{\sigma}^2/\sigma_m^2 = \hat{\sigma}^2/\sigma_a^2$ and is plotted as the "a priori" curve in Figure 8, where $\hat{\sigma}$ is taken from the dashed curves of Figure 6 and $\sigma_a = 4$ ppbv. This is considered an upper limit to the a priori scaling error, since the actual a priori value used in the retrievals is expected to be closer to the true value than an a priori of zero. *Rodgers* [1990] (see also *Marks and Rodgers* [1993]) developed an error-characterization formalism where the a priori contribution to the retrieval uncertainty is given by $\mathbf{(A–I)S}_x\mathbf{(A–I)}^T$, where $\mathbf{A}$ is the averaging kernel matrix, $\mathbf{I}$ is the unit matrix, and $\mathbf{S}_x$ is the error covariance of the quantity being retrieved. Figure 9 shows the "a priori" contribution to the uncertainty as calculated by using Rodgers' formalism and $\mathbf{S}_x$ which is diagonal with values corresponding to the 4 ppbv a priori uncertainty assumed for ClO. Figure 9 also shows the "measurement uncertainty" (that due to instrument noise) as calculated by *Rodgers* [1990] equation (17), and the total uncertainty due to combined "a priori" and "measurement." The a priori and total uncertainties calculated by this formalism are in good agreement with those from the Version 3 algorithms at 10 hPa and higher, but below 10 hPa become increasingly smaller and the difference is especially pronounced at 100 hPa. The lower-altitude differences, at least at 100 hPa, are primarily due to the inadequacies in the Version 3 algorithms for handling correlated errors.

Figure 10 shows results of simulations (without noise on the radiances) where the "true" ClO was made to cycle between 0, 1, and 2 ppbv separately at all retrieval

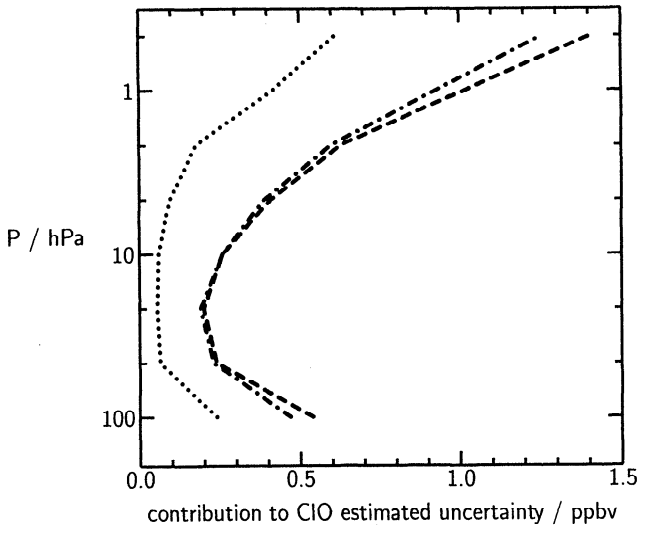

Figure 9. "A priori" (dotted) and "measurement" (dotted-dashed) contributions to uncertainties in the individual MLS ClO retrievals as calculated from the formalism of *Rodgers* [1990]. The dashed line is the combined (root-sum-square) uncertainty of these two sources.

surfaces. Except at 100 hPa (and to some extent at 0.46 hPa), where limitations of the Version 3 algorithms are expected as discussed above, the retrieval "closure" is seen (by comparing the retrieved values with the "true" values) to be within ~10%. On this basis we use 10% as an estimated scaling uncertainty due to lack of closure, and this value is shown in Figure 8.

The "P_{tan}" curve in Figure 8 is the estimated uncertainty in ClO due to 6% systematic uncertainty [*Fishbein et al.*, this issue] in the MLS tangent pressure measurement. Additional systematic uncertainties in the MLS FOV direction and shape, filter shapes, etc., are thought too small to contribute significantly to the overall scaling uncertainty for ClO. *Froidevaux et al.* [this issue] examine their effect on uncertainties in MLS ozone and conclude the worst-case effect is 5% at 100 hPa and much less at other retrieval altitudes; approximately the same percentage effects should apply to ClO as to ozone.

"Bias" Uncertainties

Bias uncertainties can be introduced in the retrievals due to lack of adequately fitting the measured radi-

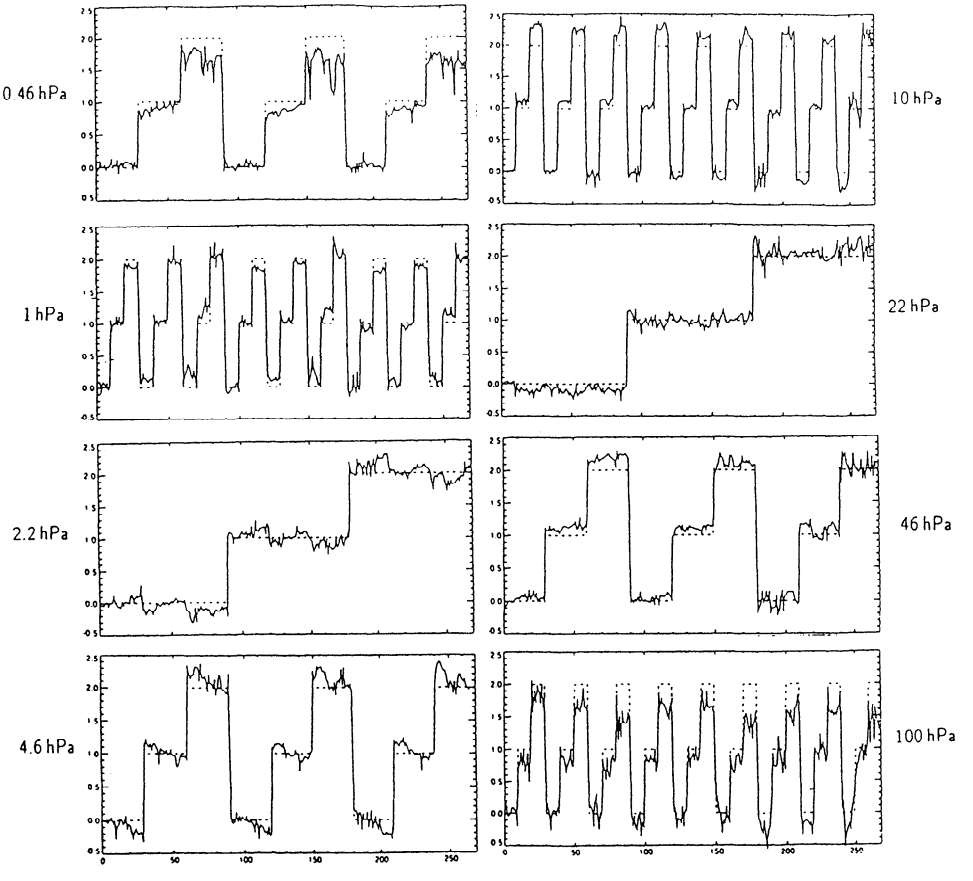

Figure 10. Results of simulations using the Version 3 ClO retrieval algorithms. The horizontal axis gives the index of individual retrievals. Dashed lines are the "truth" and solid lines are the simulated retrieval results. The "truth" was made to cycle between 0, 1, and 2 ppbv ClO at the various levels. The "noise" in the retrievals is due to other than measurement noise, as noise was not added to the simulated radiances used in these tests (although nominal radiance uncertainties were assumed by the algorithms) in order to see the effects more precisely.

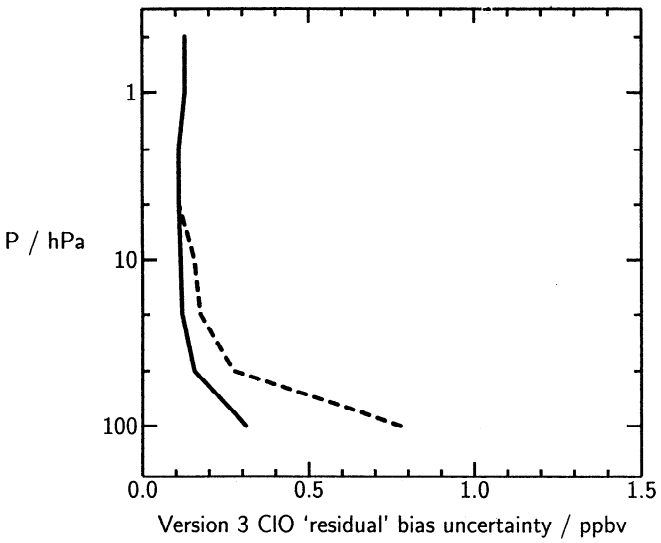

Figure 11. Bias uncertainties in Version 3 ClO (after multiplying values by 0.92; see text) due to lack of closure in fitting the measured radiances. The solid curve is for typical midlatitude ClO and the dashed curve is for enhanced lower-stratospheric ClO in the polar winter vortices.

ances by the retrieved profiles. This "residual error" can be caused by radiances from atmospheric species which are not adequately accounted for, improper modeling of certain instrumental effects, and inadequacies in the retrieval algorithms (which can also introduce "scaling" uncertainties, as discussed previously). Figure 11 shows the residual error associated with retrievals of ClO for typical midlatitude conditions and for enhanced lower-stratospheric ClO conditions encountered over Antarctica. The curves in Figure 11 were obtained by taking the differences between averages of measured radiances and averages of radiances calculated from the individually-retrieved profiles. The averaging sufficiently reduced instrument noise to where it contributed negligibly to the resulting radiance residuals. These residuals were then propagated through algorithms to determine the resulting uncertainty in ClO, which is plotted in Figure 11. Simulation tests, described below, were performed to estimate how the Version 3 "residual" uncertainties should be partitioned between "bias" and "scaling" effects.

Figure 12 shows results of simulation tests for an enhanced lower-stratospheric ClO situation. The solid curve is "truth," and radiances for the simulations were calculated from it using climatological HNO_3 and N_2O. The dashed curve gives retrievals from the Version 3 algorithms, which use the same climatological HNO_3 and N_2O; agreement with "truth" to better than 0.1 ppbv is obtained. The dotted curves in Figure 12 show results obtained from the same simulated radiances, but when HNO_3 and N_2O are changed from climatological values to zero at all altitudes. The results indicate that complete removal (at all altitudes) of HNO_3 can cause the retrieved ClO to be up to 0.4 ppbv too large at 46 hPa and 0.2 ppbv too large at 100 hPa; complete removal of N_2O can cause the retrieved ClO to be up to 0.2 ppbv too small at 100 hPa. The effect of N_2O is <0.05 ppbv at 46 hPa and above for this simulation. The effect of com-

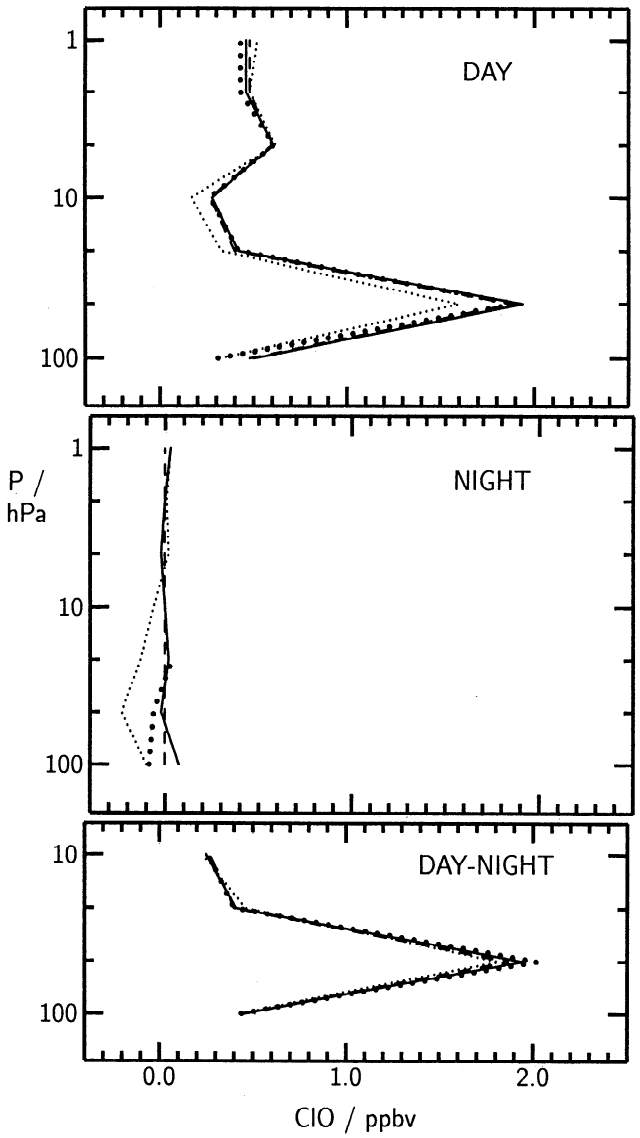

Figure 12. Results of ClO retrieval simulations for conditions of enhanced ClO in the lower stratosphere. "True profiles" are the dashed curves, from which radiances were calculated and used in simulations to produce results shown in the other curves. The solid curves give results from algorithms producing the MLS Version 3 data, which assume climatological values of HNO_3 and N_2O. The dotted curves show the effects of changing HNO_3 and N_2O between climatological profiles and zero. The curve with dense small dots is for zero HNO_3 and climatological N_2O, while that with sparse large dots is for climatological HNO_3 and zero N_2O. These results are the averages of 40 individual simulated retrievals for both "day" and "night" conditions. Curves in the bottom panel are day minus night differences for retrievals at 10 hPa and below.

plete removal of HNO_3 or N_2O on "day minus night" differences for ClO is <0.1 ppbv in this simulation test.

Figure 13 shows results from similar tests but using measured radiances. Radiances used in these tests were measured in the Antarctic vortex on 17 August and 17 September 1992. These days were chosen to be representative of (1) mid-August when MLS observes greatly enhanced ClO on both the 22- and 46-hPa retrieval surfaces and (2) mid-September when greatly enhanced ClO is present only at 46 hPa [*Waters et al.*, 1993a]. Retrievals giving largest ClO abundances were selected for examination, and the solid curves in Figure 13 are the averages of ~20 Version 3 profiles on 17 August and ~60 profiles on 17 September. The dashed curve shows results from an iterative retrieval scheme which does not have the limitations of the Version 3 algorithms and (for the same line strength) gives ~0.15 ppbv smaller values of enhanced lower-stratospheric ClO. The causes

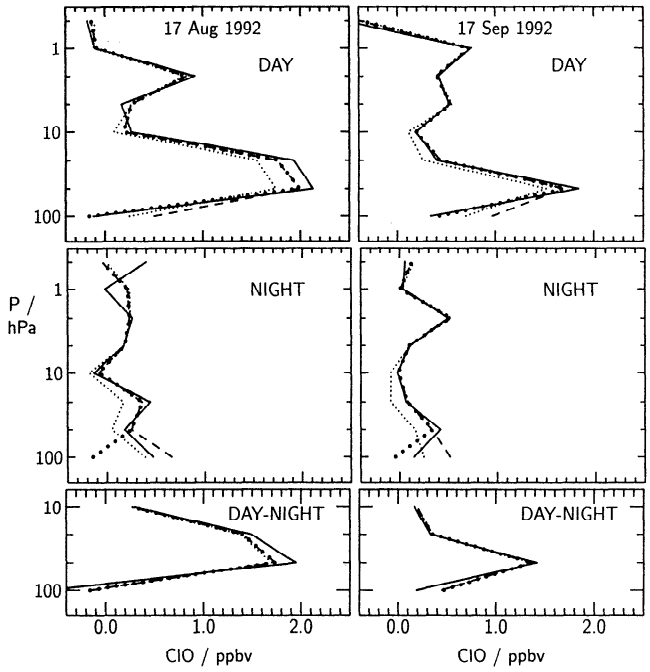

Figure 13. Results from different retrieval schemes used on MLS radiances measured over Antarctica on 17 August 1992 (left) and 17 September 1992 (right). The solid curves are MLS Version 3 data multiplied by 0.92 and are the averages of approximately 20 individual retrievals for each day. The dashed curves are from an iterative retrieval algorithm which accounts for nonlinearities and uses climatological HNO_3 and N_2O in the same way as the Version 3 algorithms. Dotted curves show the effects of changing HNO_3 and N_2O from climatological profiles to zero in the iterative retrieval. The curve with dense small dots has climatological N_2O and zero HNO_3; that with sparse large dots has zero N_2O and climatological HNO_3. The iterative results for 17 August are the averages of individual retrievals, whereas those for 17 September were obtained by a retrieval on averaged radiances from the individual limb scans. Only radiances having `MMAF_STAT=G` were included.

of this difference have been traced to differences between the atmospheric temperature and that for which the $\boldsymbol{K}$ were calculated, and to the coarseness in tabulated values of $\boldsymbol{K}$ for Version 3. This can lead to an additional +~8% Version 3 error for 46- and 22-hPa ClO in the cold polar vortices, consistent with the previously estimated 10% "closure" uncertainty for Version 3. The error due to these effects is expected to be much smaller for other altitudes and for atmospheric temperatures closer to those for which the $\boldsymbol{K}$ were calculated. A larger data set is examined below to obtain a further estimate of this error in the Version 3 data. At 100 hPa there is a discrepancy with the Version 3 values of ~0.6 ppbv for the daytime ClO profile and ~0.3 ppbv for the 17 September profiles, and problems with the Version 3 algorithms for 100-hPa retrievals have been discussed earlier. With regard to the effects of HNO_3 and N_2O on ClO, similar results are obtained as for those shown in Figure 12. The effect of setting HNO_3 to zero is to reduce the ClO peak values by ~0.4 ppbv and change the 100-hPa ClO value by ~0.5 ppbv. The effect of N_2O is less than ~0.1 ppbv at 46 hPa and above, but can be ~0.5 ppbv at 100 hPa. These differences are consistent with values expected from the residual uncertainties shown in Figure 11.

To further investigate the extent to which effects of HNO_3 contribute to uncertainties in the Version 3 ClO for the situation actually encountered in the atmosphere, we examined an ensemble of MLS measurements made during 14–29 August 1992 at locations in the Antarctic vortex where gas-phase HNO_3 was simultaneously observed to be greatly depleted [*Santee et al.*, 1995]. The HNO_3 observations used here are from preliminary versions of algorithms to be used in future reprocessing of MLS data. MLS HNO_3 is obtained primarily from its signature in the 205-GHz ozone band (see top panel of Figure 1), not from its much weaker feature which affects the ClO measurement (see bottom panel of Figure 1). This ensemble of measurements was chosen to be representative of "worst-case" effects of HNO_3 on ClO: where $\lesssim$1 ppbv HNO_3 at 46 hPa was retrieved, but the Version 3 algorithms assume ~10 ppbv HNO_3. Table 1 compares the Version 3 ClO values with those obtained when HNO_3 is also retrieved. With HNO_3 retrieved, the ClO values at 22 hPa are reduced by 0.1 ppbv and the values at 46 hPa are reduced by 0.2 ppbv, for both day and night measurements. There is insignificant change in the day-night differences at 22 and 46 hPa. The night value retrieved for ClO at 100 hPa is unchanged, but the day value is increased by 0.2 ppbv. The HNO_3 effects on 100 hPa ClO appear to arise through its effects at 46 hPa: with HNO_3 forced to climatological values, the Version 3 algorithms give (1) ~0.2 ppbv too much ClO at 46 hPa when fitting the radiances measured where 46 hPa HNO_3 is depleted, then (2) too little ClO at 100 hPa, when 46 hPa ClO is enhanced, to compensate for retrieving too large a value at 46 hPa. Table 2 compares Version 3 ClO from regions in

Table 1. Average Values of Lower Stratospheric ClO Abundances (ppbv) Retrieved From MLS Data Taken in the Antarctic Vortex During 14–29 August 1992

	Day		Night		Day minus Night	
Pressure, hPa	Version 3 ×0.92	With HNO_3 Retrieved	Version 3 ×0.92	With HNO_3 Retrieved	Version 3 ×0.92	With HNO_3 Retrieved
22	2.59±0.04	2.50±0.04	0.53±0.02	0.44±0.02	2.05±0.05	2.06±0.05
46	2.32±0.04	2.14±0.04	0.21±0.02	0.06±0.02	2.11±0.05	2.09±0.05
100	−0.34±0.07	−0.14±0.09	0.36±0.03	0.38±0.04	−0.70±0.08	−0.52±0.09

"Day" values were obtained for solar zenith angles (SZA) $\leq 83°$ at 46 and 100 hPa, and $\leq 88°$ for 22 hPa; "night" values are for SZA $\geq 100°$. The uncertainties shown here for the "day" and "night" values are the measured standard deviation of the values divided by the square root of the number of measurements which were averaged; the uncertainty given for the "day minus night" values are the root-sum-square of "day" and "night" uncertainties. The values from Version 3 have been multiplied by 0.92 to correct for the inadvertent use of an old line strength file. An additional multiplication of ~0.92, to correct for limitations of the linearized algorithms as discussed in the text, needs to be applied to these data taken within the polar vortex, both for the Version 3 values and those with HNO_3 retrieved (which also used linearized algorithms).

the January 1992 Arctic vortex where largest ClO was observed [*Waters et al.*, 1993b] with the same data set but with HNO_3 retrievals included. The effect here of HNO_3 is to slightly (~0.1 ppbv which is only marginally significant) increase the MLS Arctic enhanced ClO values. The HNO_3 retrieved from these Arctic MLS data was slightly higher than the Version 3 climatological values, as is expected due to HNO_3-rich air from evaporating polar stratospheric clouds (PSCs) in the warmer Arctic vortex.

The results described above indicate that if HNO_3 is completely removed from the atmosphere at all altitudes, then the Version 3 enhanced ClO peak abundances will be artificially large by ~0.4 ppbv. Complete

Table 2. Average Values of Lower Stratospheric ClO Abundances (ppbv) Retrieved From MLS Data Taken in the Arctic Vortex During 9–11 January 1992 Between 55°–65° N and 0–60° E

	Day		Night		Day minus Night	
Pressure, hPa	Version 3 ×0.92	With HNO_3 Retrieved	Version 3 ×0.92	With HNO_3 Retrieved	Version 3 ×0.92	With HNO_3 Retrieved
22	0.93±0.17	1.00±0.18	0.05±0.05	0.12±0.05	0.88±0.18	0.88±0.19
46	2.17±0.15	2.28±0.15	0.27±0.08	0.29±0.08	1.90±0.16	1.99±0.17
100	−0.35±0.30	−0.63±0.24	−0.02±0.16	0.01±0.15	−0.33±0.34	−0.62±0.29

"Day" values were obtained for SZA$\leq 85°$ and local solar times between 1100 and 1300. "Night" values are for SZA $\geq 120°$and local solar times between midnight and 0300. The uncertainties shown here for the "day" and "night" values are the measured standard deviation of the values divided by the square root of the number of measurements which were averaged; the uncertainty given for the "day minus night" values are the rss of "day" and "night" uncertainties. The values from Version 3 have been multiplied by 0.92 to correct for the inadvertent use of an old line strength file. An additional multiplication of ~0.92, to correct for limitations of the linearized algorithms as discussed in the text, needs to be applied to these data taken within the polar vortex, both for the Version 3 values and those with HNO_3 retrieved (which also used linearized algorithms).

removal of N_2O can affect ClO by ~0.5 ppbv at 100 hPa, but its effect at higher altitudes is negligible. For HNO_3 profiles actually encountered in the polar vortices, we expect errors in the Version 3 data of 0.1–0.2 ppbv at 22 and 46 hPa in the Antarctic and ~0.1 ppbv or less at these altitudes in the Arctic. Taking day-night differences effectively removes the bias errors due to HNO_3 and N_2O at 22 and 46 hPa.

We also applied the iterative retrieval scheme to separately averaged "day" and "night" radiances for measurements made during 14–29 August 1992 in the 65°–75° S, 0°–90° E, region of the Antarctic vortex where largest ClO was retrieved by the Version 3 algorithms; this included 178 "day" and 187 "night" retrievals. Preliminary HNO_3 retrieved from MLS was used in this iterative algorithm, and tangent pressure retrievals were obtained with an updated 63 GHz O_2 pressure-broadening parameter [*Liebe et al.*, 1992] which is 6% smaller than that used in the Version 3 retrievals (from *Liebe et al.* [1991b], essentially the same as in the work of *Liebe et al.* [1991a]). Figure 14 compares these iterative retrieval results with the average of those from Version 3 for the same measurements. The day-night differences, which should have the bias errors due to HNO_3 and N_2O removed from the Version 3 data, show 0.15 ppbv smaller values from the iterative retrievals for the enhanced ClO at 46 and 22 hPa, consistent with results shown in Figure 13 obtained from the smaller data set. Figure 15 shows the average measured radiances in the 22- to 100-hPa tangent pressure range for this data ensemble, and the averages of the radiance residuals resulting from the profiles retrieved by the Version 3 and iterative retrievals. Significantly smaller residuals are obtained with the improved iterative algorithm, as expected. From these tests we conclude that, in addition to the 8% scaling error mentioned earlier due to an "old" ClO line strength file inadvertently being used in Version 3 processing, the MLS Version 3 results for enhanced polar vortex ClO at 22 and 46 hPa are too large by (1) a bias error up to ~ +0.2 ppbv for depleted gas-phase HNO_3 conditions typical of those encountered in the Antarctic winter vortex and (2) an additional scaling error of ~ +8% due to limitations of the Version 3 algorithms. The Version 3 100-hPa ClO (including day-night differences) should not be considered reliable, at least when 46- and/or 22-hPa ClO is enhanced.

We also investigated the variation of Version 3 enhanced lower-stratospheric Antarctic ClO with respect to local solar zenith angle (SZA). Figure 16 shows enhanced ClO abundances for the same measurement ensemble as used for the results in Table 1 (Antarctic vortex during 14–29 August 1992 where gas-phase HNO_3 is greatly depleted) averaged in bins according to the SZA at the time and location of measurements (local solar time of these measurements ranged from 0800 through 2300). The variation with solar zenith angle shown in Figure 16, which includes measurements made between 60° S and 80° S, should not be interpreted as diurnal variation at a single location: the variation of SZA with latitude must be considered for quantitatively interpreting the shape of the curve, especially for values of SZA near 90°. Figure 17 shows the statistical distributions of values which went into the averages, separately for

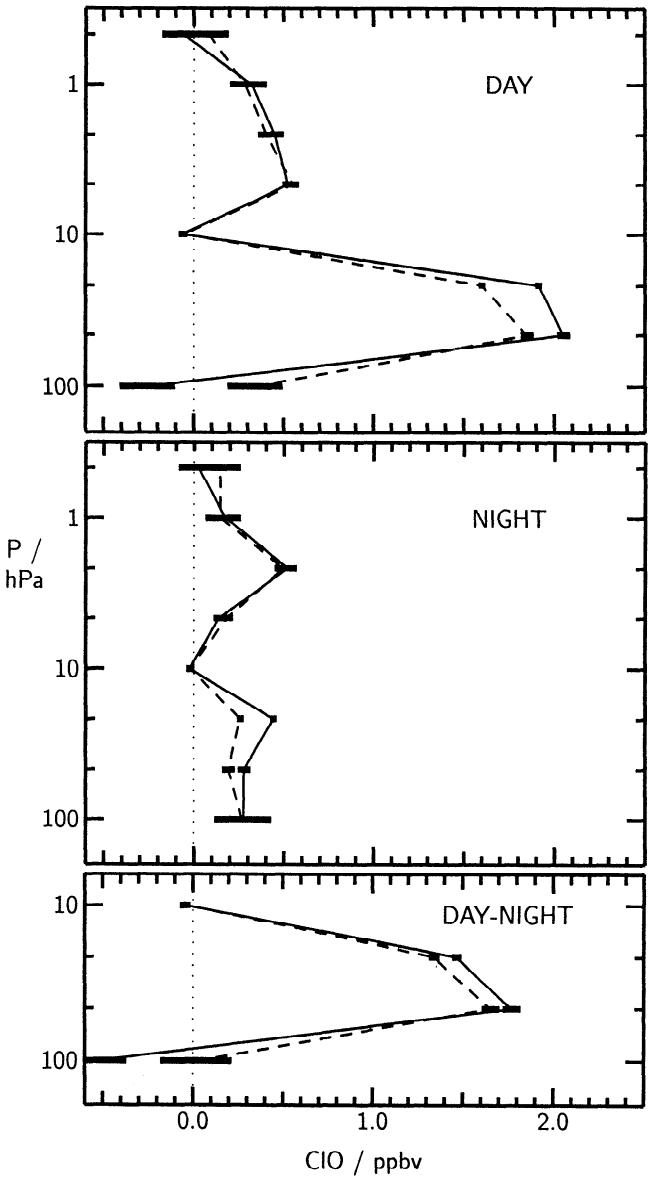

Figure 14. Average of ClO retrievals from MLS measurements made 14–29 August 1992 in the Antarctic vortex between 65°–75° S and 0°–90° E. Solid lines are from Version 3 data which have been multiplied by 0.92. Dashed lines are from an improved algorithm which accounts for nonlinearities, includes effects of HNO_3, and uses the revised O_2 linewidth parameter for retrieval of tangent pressure. Horizontal bars give the $\pm 1\sigma$ predicted precision of the averages. The "day" average consisted of 178 individual measurements which had local SZA between 78° and 91°, and local solar times between 0840 and 1440. The "night" average consisted of 187 individual measurements which had local SZA between 96° and 127°, and local solar times between 1710 and 2300. Only data having `MMAF_STAT=G` and `QUALITY_CLO=4` were included.

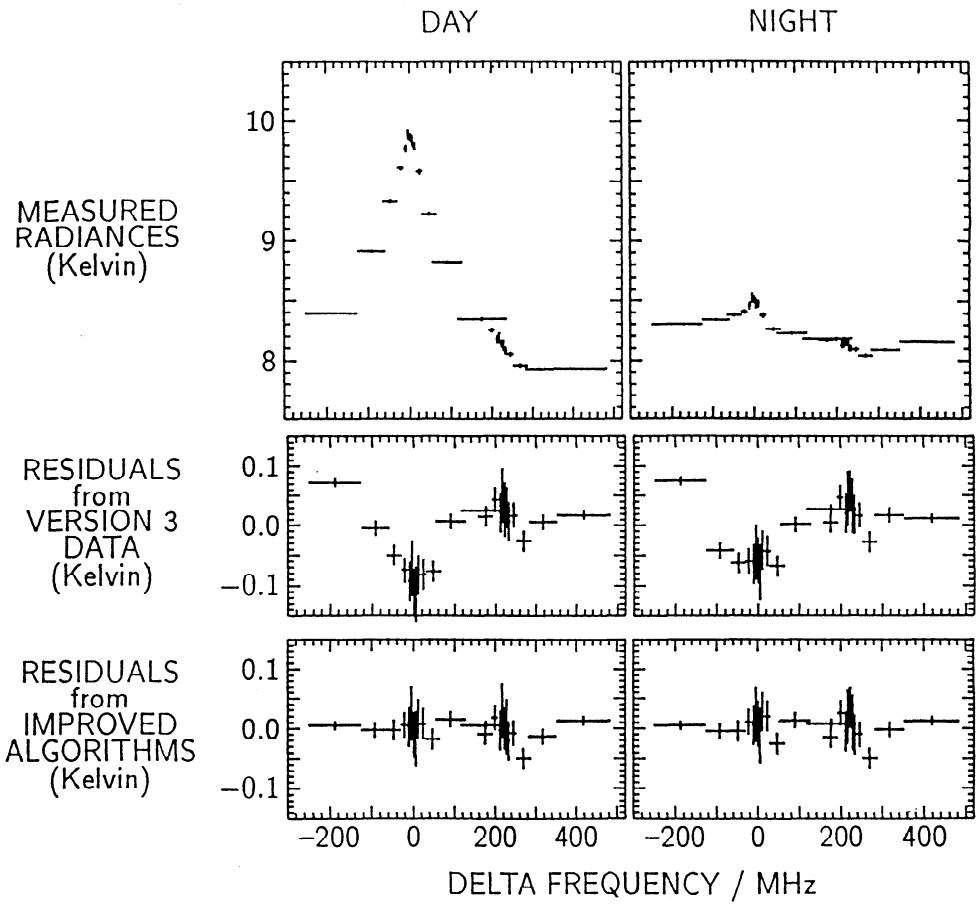

Figure 15. Averages of the radiances and residuals for the ClO retrievals shown in Figure 14. The averages are for all measurements having observation path tangent pressures between 22 and 100 hPa. Vertical bars give the estimated $\pm 1\sigma$ precision of the averages. Note that the vertical scale for the residuals has been greatly expanded from that for the measurements.

"day" and "night" measurements. The observed distribution is closely Gaussian, with width approximately equal to the uncertainty predicted by the Version 3 algorithms (except narrower than predicted at 100 hPa, as discussed earlier with regard to other data samples). This distribution suggests the samples are all from the same "population", and that it is meaningful to present averages as done for the results shown in Figure 16 and Table 1.

The variation of lower-stratospheric polar vortex ClO with solar zenith angle, when there is little available NO_2 (as should be the case for the data shown in Figure 16, since the measurements were selected where HNO_3, thought to be the dominant source of NO_2 in these circumstances, is depleted), is expected to be due to ClO-ClOOCl photochemistry, with ClO going to ClOOCl at night [e.g., *Molina and Molina*, 1987; *Solomon*, 1990]. For 3 ppbv total chlorine in ClO and ClOOCl the nighttime value of ClO calculated to be in equilibrium with ClOOCl is ~0.05 ppbv at 46 hPa (188 K) and ~0.03 ppbv at 22 hPa (180 K), where the numbers in parentheses are the average temperatures at which the measurements in Figure 16 were made. However, the expected decay after sunset at 22 hPa is sufficiently slow that equilibrium is not expected to be reached at the time past sunset (0–7 hours) at which the measurements in Figure 16 were made, and ~0.4 ppbv ClO at 22 hPa is expected for the largest solar zenith angles shown in Figure 16. Averages of MLS measurements made well into the polar night (not shown here) give smaller 22-hPa ClO abundances of ~0.1 ppbv, in better agreement with the expected equilibrium values. The nighttime ClO values at 22 and 46 hPa in Figure 16 thus appear, within their uncertainties, to be consistent with expected behavior. The Version 3 100-hPa ClO behavior with respect to solar zenith angle shown in Figure 16 is unrealistic, and an artifact due to the Version 3 algorithm limitations mentioned above.

The daytime 46- and 22-hPa values shown in Figure 16 are typical of the largest ClO abundances observed by MLS. After accounting for the 8% scaling error in Version 3 data due to inadvertent use of the "old" line strength file (already done in Figure 16), the additional ~8% scaling error at 46 and 22 hPa due to algorithm limitations, and the estimated bias error of 0.2 ppbv due to HNO_3, the maximum values become

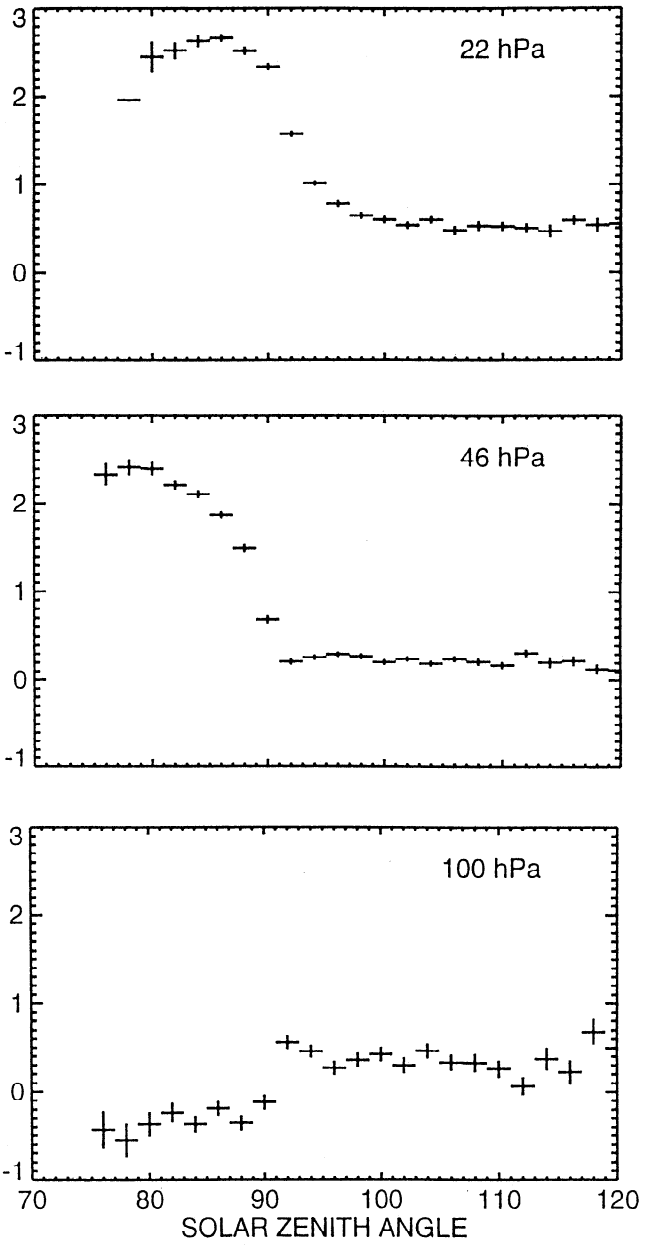

Figure 16. Retrieved lower-stratospheric ClO as a function of zenith angle, for time and location of largest ClO abundances measured by MLS (Version 3 data, multiplied by 0.92). Shown here are averages of measurements made in the Antarctic vortex during 14–29 August 1992, and are plotted as a function of SZA at the time and location of the measurements. The data were selected where MLS observed greatly depleted HNO_3 and cover latitudes 60°–80° S; it should be emphasized that these curves do not represent ClO diurnal variation at a single location and that variation with latitude must be considered for their proper scientific interpretation. The vertical scale is ppbv and the data have been averaged in 2° SZA bins; only data with `MMAF_STAT=0` and `QUALITY_CLO=4` have been included. As discussed in the text, the unrealistic behavior in 100 hPa ClO is an artifact and peak ClO values at 46 and 22 hPa become 2.0±0.2 and 2.3±0.2 ppbv, respectively, after accounting for effects caused by HNO_3 and Version 3 algorithm limitations.

2.0 ppbv at 46 hPa and 2.3 ppbv at 22 hPa, with an estimated uncertainty of ~0.2 ppbv. These values, if interpreted as ClO abundances at the indicated pressures, imply 3.4±0.5 ppbv total chlorine in ClO and ClOOCl at 46 hPa and 2.7±0.3 ppbv at 22 hPa (using nominal rate parameters for ClO-ClOOCl photochemistry [*DeMore et al.*, 1994; *Nickolaisen et al.*, 1994]), where the uncertainties given here do not include uncertainties in the photochemical parameters. The maximum values implied for ClO+ClOOCl are just within the 3.4±0.3 ppbv total stratospheric chlorine measured in 1992 by the ATMOS experiment [*Gunson et al.*, 1994] and indicate that most of the chlorine in the lower stratosphere was in ClO and ClOOCl during the time and location of these MLS measurements. More work is needed to account for effects of the MLS vertical resolution on the implications of its ClO measurements for the total chlorine in ClO and ClOOCl.

To investigate the solar zenith angle behavior of Version 3 ClO when lower-stratospheric ClO is not greatly enhanced, averages of summer measurements of ClO binned by solar zenith angle were performed, and the results are shown in Figure 18. The large artifacts in 100-hPa ClO which appear in the Antarctic vortex data, when 22- and/or 46-hPa ClO is enhanced, are not present in these data. The retrieved summer 100 hPa ClO values are zero to within the ~0.05 ppbv noise level of the averages. Unrealistic negative values of ~0.1–0.2 ppbv (which are outside the expected noise of the averaged points), however, appear in nighttime values at 10–46 hPa. Figure 19 shows average profiles retrieved from measurements taken between midnight and sunrise during summer in both hemispheres. Between 100 and ~4.6 hPa we expect ClO to be essentially zero between midnight and sunrise, so we interpret the negative values in the averages at these altitudes as a bias error in the retrievals. Their magnitude is consistent with the expected residual uncertainties shown in Figure 11. The ClO is not expected to decrease so much at night at higher altitudes, and this is seen in the MLS data shown in Figure 18. The model results of *Ko and Sze* [1984] predict midnight ClO to be (1) ~2× lower than midday ClO at 2 hPa, (2) essentially the same as midday ClO at 1 hPa, and (3) ~0.1 ppbv larger than midday ClO at 0.46 hPa. The MLS results shown in Figure 18 agree reasonably well with these predictions. Figure 20 shows averages of radiances measured near noon and midnight for tangent pressures of 0.46–1.0 hPa and 1.0–2.2 hPa, and for 4 days during the period which the data for Figure 18 were obtained. The ClO spectral feature is clearly present in both the noon and the midnight spectra at 1.0–2.2 hPa. However, the feature is not so clear in the 0.46- to 1.0-hPa radiances, and more investigation is needed before the 0.46 hPa ClO retrievals can be considered adequate for general scientific analyses. Improvements in Level 1 processing for future versions of the MLS data are expected to improve the quality of the high-altitude radiances.

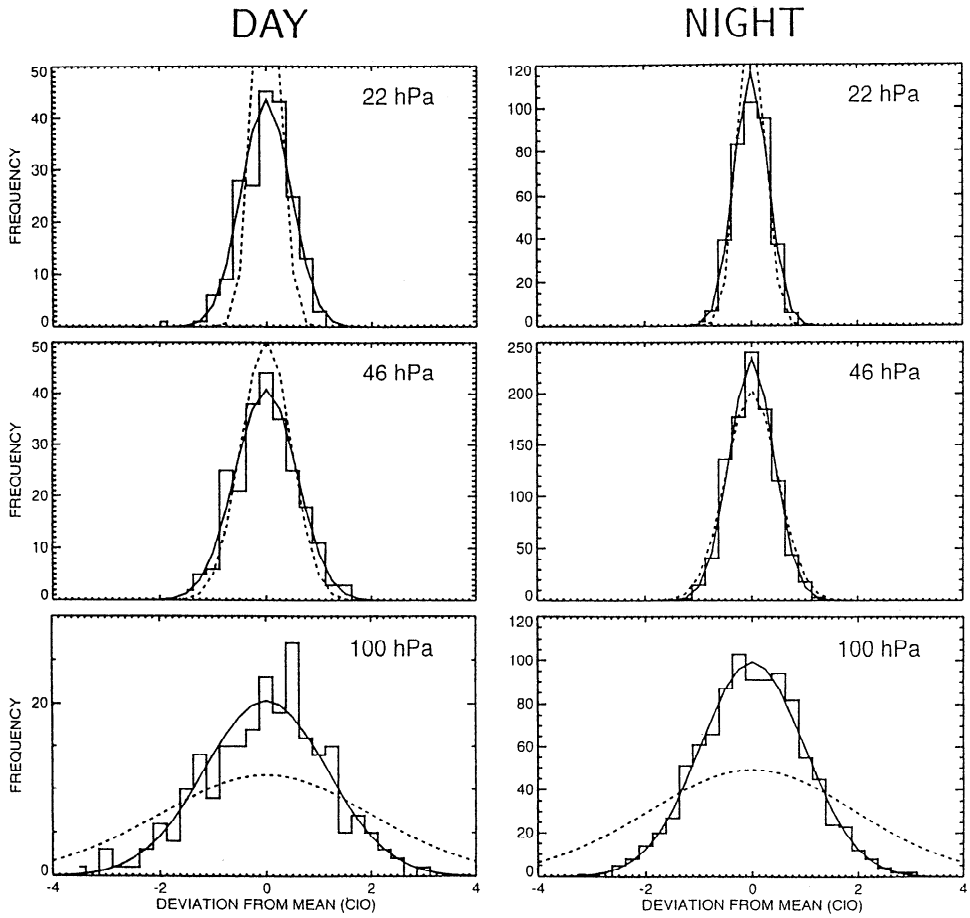

Figure 17. Statistical distribution of the ClO values (Version 3, multiplied by 0.92) which have been averaged for Figure 16. "Day" is defined as SZA$\leq$83° for 46 and 100 hPa, and $\leq$88° for 22 hPa. "Night" is defined as SZA$\geq$100°. The horizontal axis is variation from the mean in ppbv; the vertical axis is number of occurrences of that value. Histograms give the distribution of retrieved values, binned in 0.25 ppbv increments. The smooth curves are Gaussians having approximately the same enclosed area as the histograms. The solid Gaussian has width equal to the measured standard deviation of the data, and the dashed has width equal to the average of the uncertainties predicted by the Version 3 algorithms.

Summary of Estimated Uncertainties

Table 3 summarizes our estimates for the three types of uncertainties for the Version 3 ClO data and known problems in these data, based on the analyses described above. Figure 21 gives a plot of the estimated uncertainties. The "noise" uncertainties shown in Figure 21 are typical 1σ values for a single profile; uncertainties given in the data files should be used for the noise on any specific individual retrieval. Values for the bias uncertainties given here are based on the residual uncertainties in Figure 11 but have been increased by $\sim$0.05 ppbv due to non-physical negative nighttime values at 22 hPa (see Figure 19) being up to 0.05 ppbv larger than the uncertainties shown in Figure 11. Values for the "scaling uncertainties" are the root-sum-square of values in Figure 8, with the result rounded up to the nearest 5%. These apply to the Version 3 data after they have been multiplied by 0.92 to correct for the error in using an "old" line strength file during Version 3 processing. We believe the systematic "bias" and "scaling" uncertainties given here represent envelopes which are not often exceeded, that they are roughly 90% confidence (2σ) values.

6. Comparisons With Other Measurements

We now compare MLS results for ClO with those from other measurement techniques. Useful comparisons generally require averaging of MLS results because of the low signal-to-noise on individual retrievals of ClO.

Comparisons With Balloon Measurements

Many pre-UARS measurements of upper-stratospheric ClO were made from balloons at northern hemisphere midlatitudes. Figure 22 shows 20°–40° N monthly zonal mean midday profiles from MLS for every north-looking UARS month from October 1991 through August 1993.

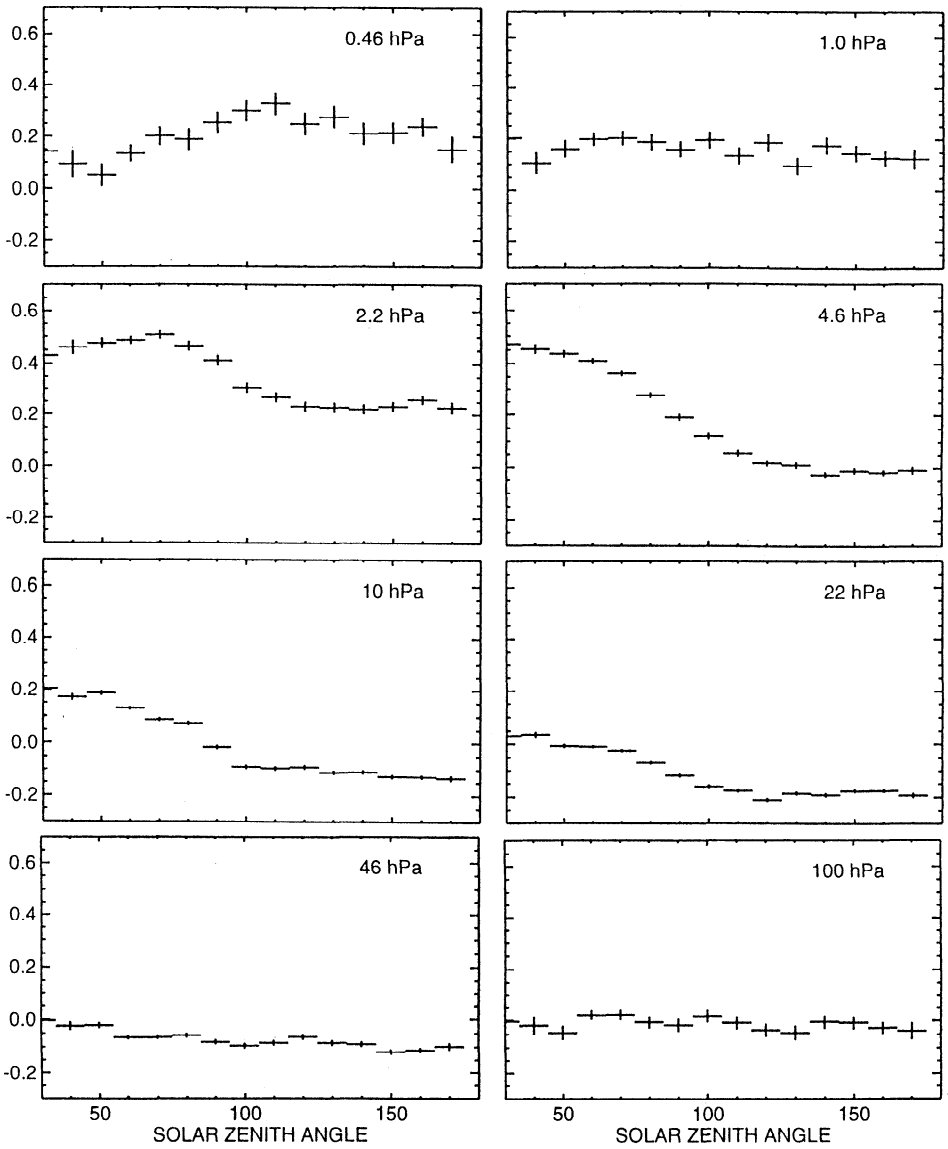

Figure 18. Variation with SZA of MLS ClO measurements made during the summer south-looking period from 15 January to 14 February 1992 (Version 3 data, multiplied by 0.92). Individual retrievals were binned by SZA, and then averaged over all latitudes (80°S to 34°N) to produce the results shown here. The vertical scale is ppbv, and vertical bars show the expected precision of the average. Only data having `MMAF_STAT=G` and `QUALITY_CLO=4` have been included.

The variation in these monthly zonal means is seen to be small ($\lesssim$0.1 ppbv), suggesting that useful comparisons of midlatitude upper-stratospheric ClO can be made without regard to the particular season of the measurements. Figure 23 compares the MLS monthly zonal means with the summary of midlatitude upper-stratospheric ClO measurements given by *Waters et al.* [1988]. There is general agreement to ~0.1 ppbv below 35 km, but some of the earlier measurements shown in Figure 23 give significantly more ClO above ~35 km (up to 0.9 ppbv at 40 km, ~0.4 ppbv more than MLS) than appear in the MLS monthly zonal means. Even larger values of upper-stratospheric ClO were obtained on individual midlatitude balloon flights, up to ~9 ppbv measured at 41 km on 14 July 1977 [*Weinstock et al.*, 1981], but such large values do not appear in the MLS zonal means; if real, they must be, as concluded by *Weinstock et al.* [1981], anomalous situations which are not representative of typical conditions. Examination of all ~10^6 individual MLS ClO retrievals from the first 3 years of measurements, which meet the objective quality criteria discussed earlier (more than 99.9% of the total number), have shown no ClO values at 2.2 or 4.6 hPa (~36–42 km) which are significantly greater than the ~3 ppbv peak noise of individually-retrieved values at these altitudes. We note that no adjustments have been made for the increase in stratospheric chlorine between the times of MLS and earlier balloon measurements shown in Figure 23, and that accounting for this would only exacerbate the differences between MLS

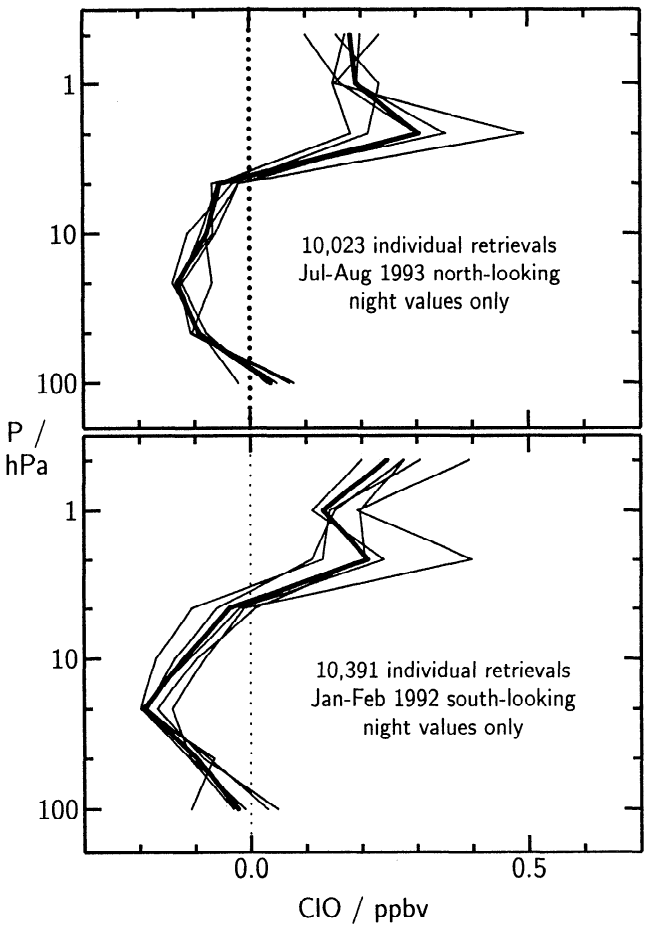

Figure 19. Averages of nighttime ClO retrievals. These are Version 3 data taken during (top panel) the 9 July through 7 August 1993 north-looking period, and (bottom panel) the 15 January through 14 February 1992 south-looking period; all have been multiplied by 0.92 as discussed in the text. Only measurements made in early morning (local solar times between midnight and 0600; SZA>95°) and those having `MMAF_STAT=G` and `QUALITY_CLO=4` were included. The thick line gives averages of all data (more than 10,000 individual retrievals from each of the hemispheres). Thin lines give 20° wide zonal averages in separate latitude ranges.

and some of the early upper-stratospheric ClO measurements.

Figure 24 shows balloon measurements of ClO made during March and April 1991 at 34° N by the Submillimeter Limb Sounder (SLS) [*Stachnik et al.*, 1992] and by the *in situ* technique [*Avallone et al.*, 1993a]. These are compared with 30°–40° N MLS zonal means (day-night differences) for the MLS north-looking periods in February and March 1992, 1993, and 1994. The agreement among all three techniques is better than 0.1 ppbv at all altitudes. MLS shows slightly larger ClO abundances at 46 hPa (~21 km), which is only marginally significant relative to the expected uncertainty. Such an increase could be due to effects of the Pinatubo volcano which erupted between the sets of measurements. *Avallone et al.* [1993b] have analyzed aircraft *in situ* data and show ~0.03 ppbv increase in ClO at ~50 hPa and 30° 40° N between February 1989 data taken before Pinatubo and that taken in February 1992 after Pinatubo (when the first set of MLS measurements shown in Figure 24 were made), and this increase is approximately the amount by which MLS is larger. Comparisons of MLS results with those from aircraft are in a later subsection of this paper.

ClO profiles coincident with MLS were measured by the balloon-borne SLS as part of the UARS correlative measurements program. SLS measurements at the same time as MLS were obtained on 1 October 1991 (launched from Fort Sumner, New Mexico, 34° N), 20 February 1992 (Daggett, California, 35° N), 29 September 1992 (Fort Sumner) and 3 April 1993 (Daggett). The estimated SLS accuracy is 0.1 ppbv or better over a vertical range between 50 and 1 hPa. Figure 25 compares MLS 30°–40° N zonal mean ClO profiles with those measured on individual flights of SLS. The daily zonal means from MLS agree, to within the estimated uncertainties, with the SLS profiles over the full vertical range of the measurements. The MLS monthly zonal means agree to within ~0.1 ppbv or better with SLS over the full vertical range. The 3 April 1993 SLS flight occurred when MLS was looking south, so that MLS profiles are not available on that date for comparison (measurements at the northern extreme of the south-looking orbit were in darkness); data from that flight are included below (Figure 34) in a time series of MLS data.

Comparisons With Ground-Based Measurements

Ground-based measurements of stratospheric ClO were first reported by *Parrish et al.* [1981], and typical midlatitude results obtained prior to UARS are given in the curve labeled "Barrett et al." in Figure 23. Measured variation in upper-stratospheric ClO throughout a complete diurnal cycle over Hawaii (19° N) during October and December 1982 was reported by *Solomon et al.* [1984]. Figure 26 compares the *Solomon et al.* [1984] results with the 10°–30° N zonal mean diurnal variation observed by MLS during the UARS north-looking months of October 1992 and December 1991. The ClO column abundance above 30 km inferred from the ground-based measurement is shown, along with the column above 10 hPa from MLS. The model [*Ko and Sze*, 1984] predictions given by *Solomon et al.* [1984] are also included in Figure 26. Both the measurements and the model results have been normalized in the same manner. There is generally good agreement between MLS and ground-based measurement but with the MLS measurements fitting more closely the model predictions of a steeper morning rise than is evident in the ground-based measurements. The midday column above 30 km from the ground-based measurements is $0.7–0.8\times10^{18}$ molecules/m^2, whereas that inferred from MLS (Version 3 data multiplied by 0.92) is $0.9–1.1\times10^{18}$ molecules/m^2. The difference of 35±20% is consistent,

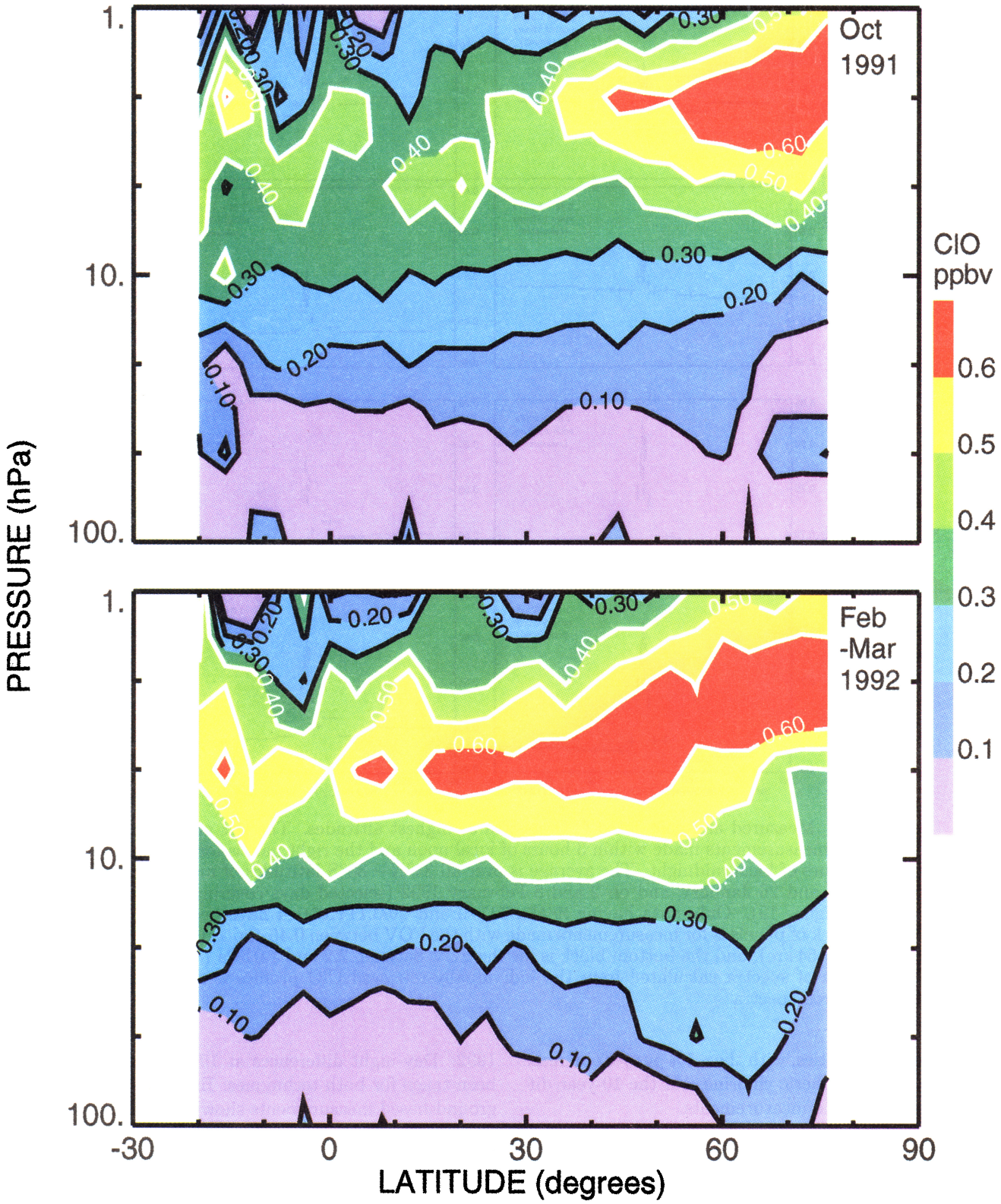

Plate 2. Zonal mean of MLS daytime ClO measurements for (top) 1 to 31 October 1991 and (bottom) 15 February to 22 March 1992. The latitude interval is 4° and each latitude bin is an independent sample (i.e., there has been no "smoothing" of the results). The data are Version 3 multiplied by 0.92, and only records having `MMAF_STAT=G` and `QUALITY_CLO=4` have been included. Day-night differences have been taken at 4.6 hPa and below.

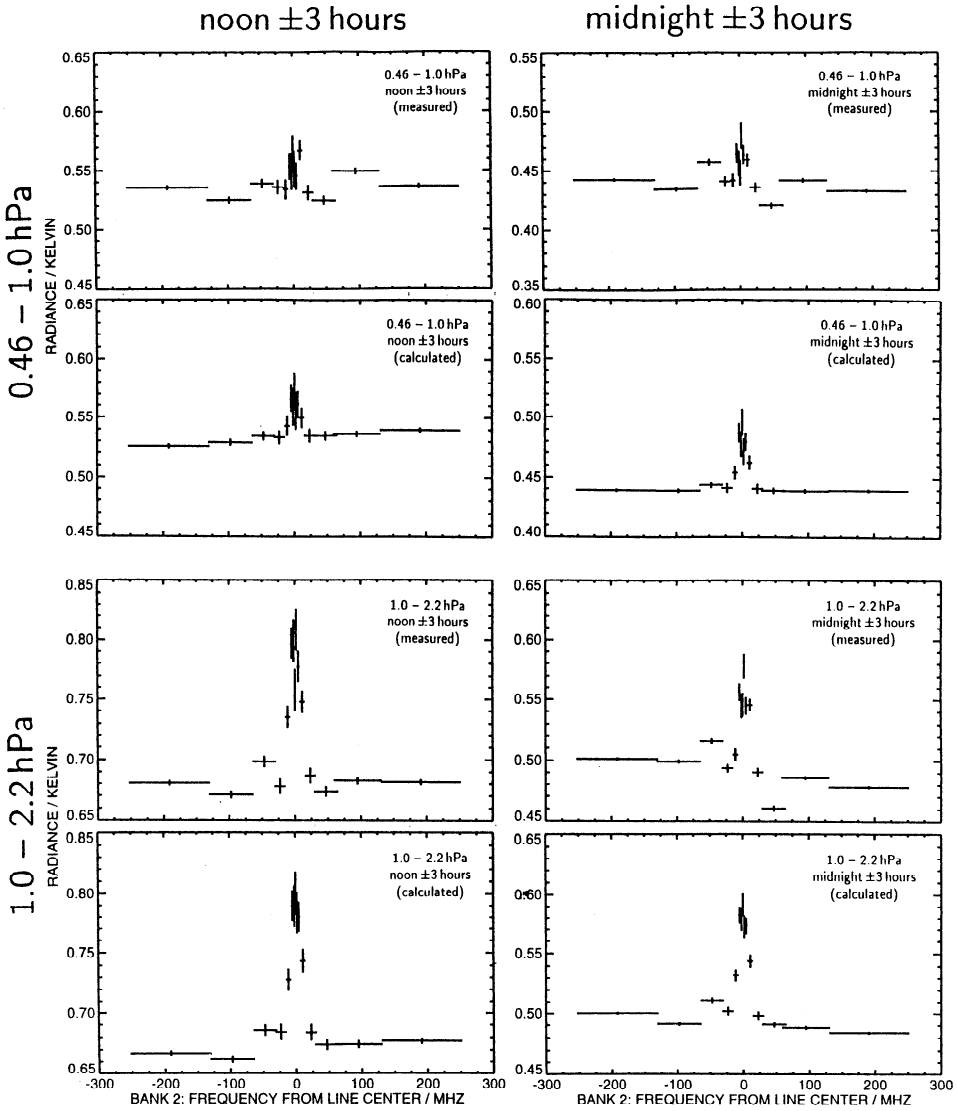

Figure 20. Measured and calculated ClO spectra at highest altitudes. The left panels are for averages of measurements made within 3 hours of local noon and the right panels for those made within 3 hours of local midnight. The average is over all 34°N – 80°S latitudes of measurements made on 19 and 26 January, and on 2 and 8 February 1992 (selected days covering the period shown in Figure 19). Only data having `MMAF_STAT=G` and `QUALITY_CLO=4` have been included. The top block of panels is for measurements made with the FOV between 0.46 and 1.0 hPa tangent height (~48–54 km), and the bottom block is for the FOV between 2.2 and 1.0 hPa (~42–48 km). The average of spectra calculated from the individually-retrieved ClO profiles is shown below each measured spectra.

within the uncertainties, with the ~5% per year increase expected in stratospheric chlorine and the 10-year difference in time of the measurements.

Enhanced ClO in the lower stratosphere over Antarctica has been measured by ground-based microwave radiometers operating at McMurdo Station (78°S, 166°E) since 1986 [*deZafra et al.*, 1987; *Solomon et al.*, 1987; *Barrett et al.*, 1988; *deZafra et al.*, 1989]. This technique has also been used as part of the UARS correlative measurements program to obtain ClO measurements from McMurdo at the same time as MLS. Figure 27 compares MLS and ground-based [*Emmons et al.*, 1995] ClO measurements over McMurdo during 15–20 September 1992. Day-night differences at 10 hPa and below have been taken for both techniques. Both the MLS and the ground-based measurements show the "double-peaked" ClO profile, which is caused by separate regimes of gas-phase chemistry in the upper stratosphere and heterogeneous chemistry in the lower stratosphere. The heights of the ClO peaks obtained from the two techniques are in good agreement, and the peak abundances agree to within ~0.1 ppbv and the expected uncertainties. There are differences of ~0.2 ppbv at 22–30 km which may be due to the different spatial resolution of the two techniques and the different methods used for representing the vertical variation.

Table 3. Summary of Estimated Uncertainties and Known Artifacts in MLS Version 3 ClO

Pressure, hPa	Typical Single Profile 1σ Noise, ppbv	Estimated Bias Uncertainty, ppbv	Estimated Scaling Uncertainty, %	Known Artifacts*
0.46	1.5	0.2	20	More investigations are required before the Version 3 0.46-hPa values can be considered sufficiently reliable for general scientific analyses.
1.0	1.2	0.2	15	
2.2	0.7	0.15	15	
4.6	0.5	0.15	15	Version 3 data have a bias error of –0.05 ppbv
10	0.4	0.15	15	Version 3 data have a bias error of –0.1 ppbv
22	0.3	0.2	15	Version 3 data have a bias error of –0.15 to –0.2 ppbv when HNO_3 has typical 'climatological' values, and a bias error of ~+0.2 ppbv under conditions of depleted HNO_3 typical of the Antarctic vortex; these bias errors can be removed by taking day-night differences, when conditions permit. There is an additional scaling error of ~+8%, due to Version 3 algorithm limitations, for enhanced ClO in the polar winter vortices (see text).
46	0.4	0.2–0.4	15	Version 3 data have a bias error of –0.1 ppbv when HNO_3 has typical 'climatological' values, and a bias error of ~+0.2 ppbv under conditions of depleted HNO_3 typical of the Antarctic vortex; these bias errors can be removed by taking day-night differences (when conditions permit). There is an additional scaling error of ~+8%, due to Version 3 algorithm limitations, for enhanced ClO in the polar winter vortices (see text).
100	1.0	0.4–0.8	25	Version 3 100-hPa data are not reliable under conditions when 22- and/or 46-hPa ClO is greatly enhanced. More investigations are required before they can generally be considered reliable at the small ClO abundances which are typically expected at 100 hPa

The "noise" uncertainty gives the "precision" of the measurement and can be reduced by averaging. The values given here for the "bias" and "scaling" uncertainties, which apply to the "accuracy" of the measurements after accounting for noise, are believed to represent envelopes which are not often exceeded, roughly 90% confidence (2σ) values; they apply to the Version 3 data after values have been multiplied by 0.92.

*All Version 3 ClO values should be multiplied by 0.92 to account for incorrect ClO line strength used in the production of these data. Additional pressure-dependent artifacts are listed.

Figure 28 compares the ClO profiles obtained from ground-based [*deZafra et al.*, 1995] and MLS measurements over McMurdo during 4–7 and 15–17 September 1993. Both measurements show more lower-stratospheric ClO over McMurdo in 1993 than in 1992, especially at ~22 km (~22 hPa) altitude and in the thickness of this lower layer. More ClO over McMurdo in 1993 than in 1992 at these times is expected from the differences in vortex location between 1992 and 1993 for the periods shown in Figures 27 and 28. MLS maps of ClO for this period (unpublished results) and those of potential vorticity [*Manney et al.*, 1993; 1995b] show

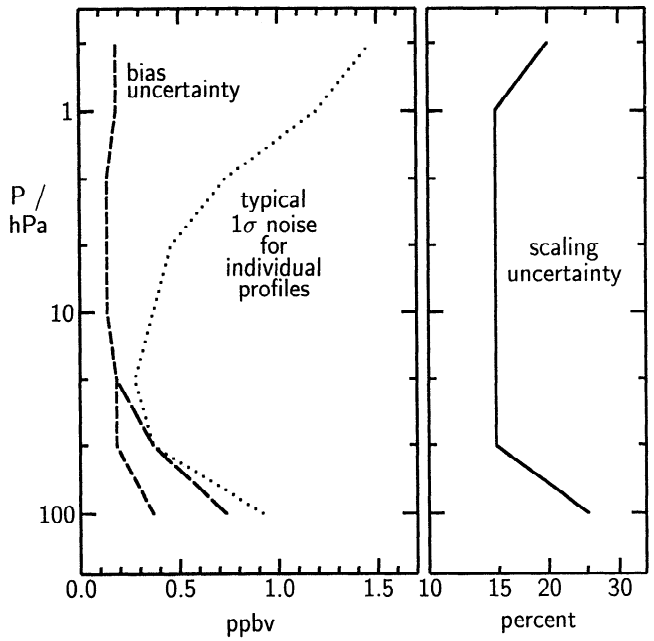

Figure 21. Summary of estimated noise (dotted line), bias (dashed lines), and scaling (solid line) uncertainties for MLS Version 3 ClO (after the Version 3 values have been multiplied by 0.92 as discussed in the text). The short-dashed curve is for typical midlatitude ClO and the long-dashed curve is for conditions of enhanced lower-stratospheric ClO in the polar winter vortices. The curves for the "bias" and "scaling" uncertainties are believed to represent envelopes which are not often exceeded, roughly 90% confidence (2σ) values.

the region of largest lower-stratospheric ClO, and the Antarctic vortex, extending further outward over McMurdo for the periods shown in Figure 28 than for that shown in Figure 27. These maps also show the Antarctic lower-stratospheric vortex and region of enhanced ClO to be more distorted toward McMurdo during 15–17 September 1993 when the air over McMurdo was representative of that deeper within the vortex than during 4–7 September 1993 (see also Figure 4 of *deZafra et al.* [1995]). MLS shows 46-hPa ClO increasing from 4–7 September 1993 to 15–17 September 1993, as might be expected from the changes in vortex location between these periods. To ensure the increase observed by MLS was not an artifact of the retrieval technique, retrievals were performed on the same data set but with the radiances first averaged and the iterative retrieval performed on the averaged radiances. Results from the radiance-averaged iterative retrieval are the thick dashed lines in Figure 28. The same temporal increase is seen at 46 hPa as in the Version 3 MLS data, although lower-stratospheric ClO peak abundances are ~0.2 ppbv smaller, consistent with tests described earlier. Both the MLS and the ground-based measurements show the peak of the lower-stratospheric ClO layer to decrease in altitude between 4–7 and 15–17 September. There is a discrepancy of ~0.5 ppbv at 10 hPa, where MLS shows less ClO than the ground-based measurement, and this is likely due to the differing vertical resolutions of the two techniques. Analyses have indicated the ground-based technique should not, in the presence of greatly enhanced lower-stratospheric ClO, be expected to resolve the relatively narrow "notch" in ClO seen by MLS at ~10 hPa, whereas MLS should be able to do so.

Figure 29 shows column measurements of ClO over Thule, Greenland, during February and March 1992 [*deZafra et al.*, 1994] and compares these with columns obtained from MLS. The ground-based measurements were taken during midday and are averages over periods of 3–5 days. Column ClO computed from individual MLS measurements made nearest Thule on both the ascending and the descending portions of the orbit are shown, and the MLS data have been smoothed with a 5-day running average. During the period of these comparisons the "day" side of the orbit for MLS measurements slowly changed from ascending to descending, and the solar zenith angle and local solar time of the MLS measurements are given in the two bottom panels. Maps of potential vorticity (G.L. Manney, private communication, 1995) show that during late February and up until ~5 March stratospheric air over Thule was well inside the Arctic polar vortex, but it was near the vortex edge after ~5 March; on 17–18 March the vortex was located more over Thule than on adjacent days. This behavior can be seen in the time series of potential vorticity over Thule shown in Figure 4 of *Emmons et al.* [1994] who discuss vortex dynamics and ground-based N_2O observations over Thule during this period. The

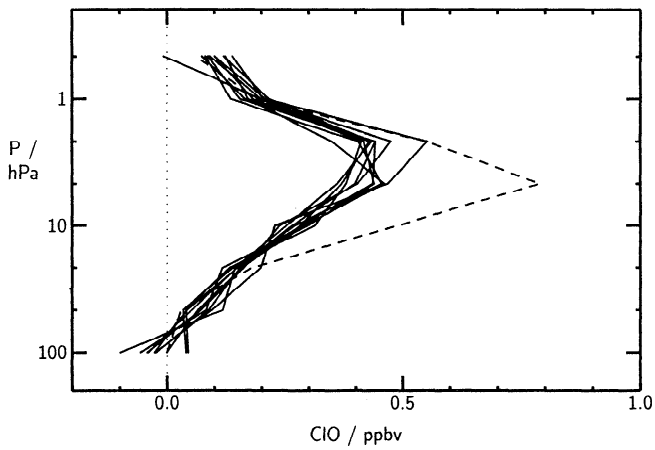

Figure 22. The 20°–40° N monthly zonal averages of ClO profiles from MLS (solid lines) for all north-looking UARS months from September 1991 through August 1993. These are Version 3 data multiplied by 0.92; only data taken at SZA<80° and with local solar times between 0900 and 1500 were included in the average. Values from the night side of the orbit (SZA>95°) have been subtracted at 10 hPa and greater pressures to remove $\lesssim$0.2 ppbv bias errors as discussed in the text. Only data having `MMAF_STAT=G` and `QUALITY_CLO=4` were included in the averages. The dashed line shows the a priori profile used by the retrieval algorithms.

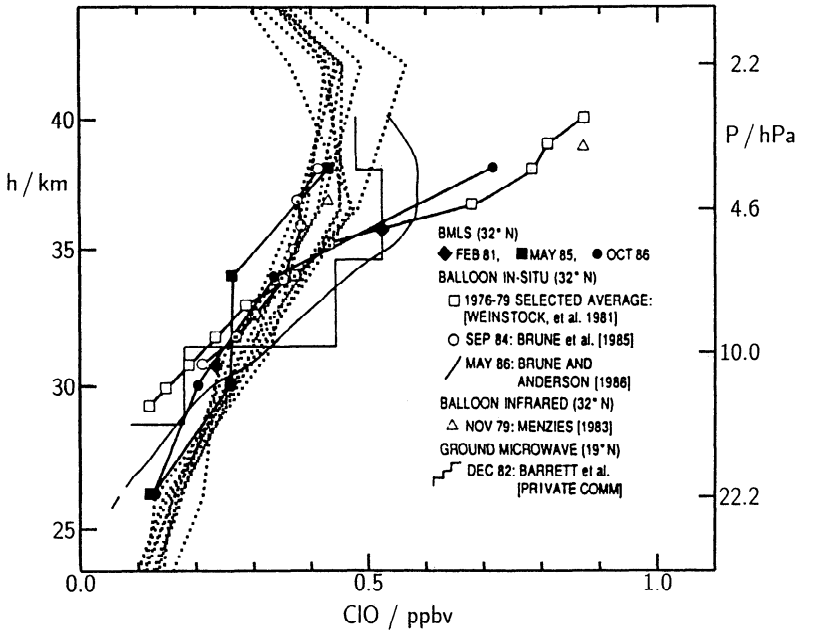

Figure 23. Comparison of MLS 20°–40° N zonal mean ClO profiles with pre-UARS profiles measured at these latitudes, as summarized in Figure 3 of *Waters et al.* [1988]. The MLS profiles are dotted and are the same as those shown over a larger vertical range in Figure 22.

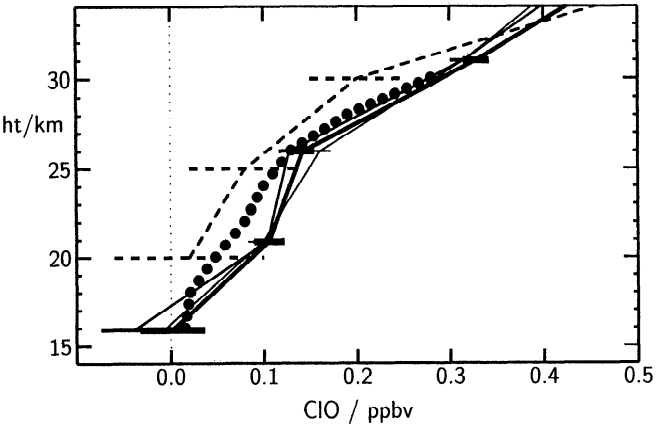

Figure 24. Comparison of 30°–40° N lower-stratospheric ClO zonal means from MLS north-looking periods 15 February to 23 March 1992 (thin lines), 10 February to 19 March 1993 (medium lines) and 5 February to 14 March 1994 (thick lines) with balloon Submillimeter Limb Sounder (SLS) [*Stachnik et al.*, 1992] (dashed lines) and *in situ* [*Avallone et al.*, 1993a] (points) measurements for approximately the same time of year in 1991. The MLS values are day-night differences, with "day" measurements having SZA<80°, and "night" measurements having SZA>110°; Version 3 data multiplied by 0.92 are shown here. Approximately 1200 individual MLS profiles were averaged for day and for night, including only data with `MMAF_STAT=G` and `QUALITY_CLO=4`. The horizontal extents of the bars for the MLS are the observed standard deviation of the retrieved values divided by the square root of the number of measurements (and root-sum-squared for the day-night difference).

agreement between MLS and ground-based ClO observations is good, and within the combined uncertainties of the techniques, during the early portion of the period when Thule is well under the vortex. The degradation during the latter portion when Thule is under the edge of the vortex is possibly due to the two measurements' different spatial and temporal sampling, whose effects should be more pronounced in a more dynamically variable situation as occurs near the vortex edge.

Figure 30 compares MLS and ground-based [*Shindell et al.*, 1994] measurements of the ClO profile over Thule during February and March 1993. Both measurements show the lower-stratospheric ClO abundance to decrease between 21–24 February and 13–19 March 1993, and there is agreement in the ClO abundances at the peaks of both the lower-stratospheric and the upper-stratospheric layers to within ~0.1 ppbv. Differences in the heights of the profile peaks may be due to the differing vertical resolutions of the two techniques, as discussed earlier.

Ground-based column measurements of HCl over Åre, Sweden (63° N), performed as part of the EASOE campaign [*Pyle et al.*, 1994] during the 1991–1992 Arctic winter, have been compared with ClO columns over Åre during the same period [*Bell et al.*, 1994]. During early January 1992, when MLS observed a large increase in ClO, the HCl column was greatly decreased as expected, since the January increase in ClO should be at the expense of HCl.

Comparisons With Aircraft Measurements

Enhanced lower-stratospheric ClO was measured from the ER-2 aircraft during the 1987 Antarctic campaign

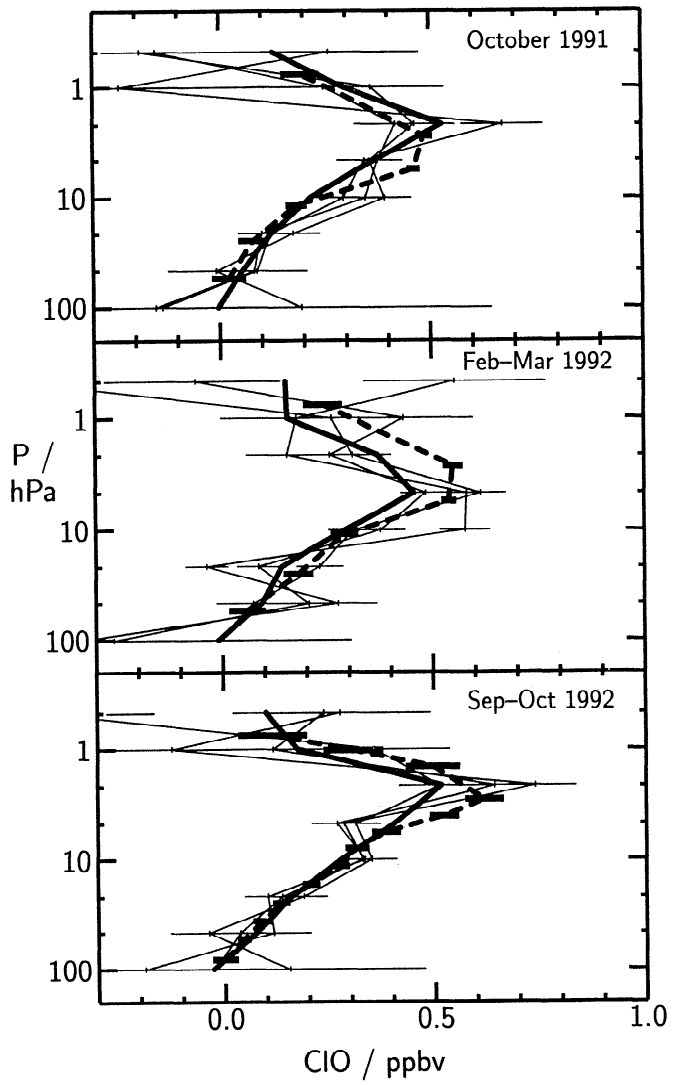

Figure 25. Comparison of SLS ClO measurements (dashed lines) at ~35° N with 30°–40° N zonal mean ClO measured by MLS (solid lines) during the same time periods as SLS: (top) on 1 October 1991 from Fort Sumner, New Mexico; (middle) on 20 February 1992 from Daggett, California; (bottom) on 29 September 1992 from Fort Sumner. All measurements were made during midday, and ClO values from the "night" side of the orbit have been subtracted from the MLS data at 10 hPa and greater pressures to remove known biases of 0.1–0.2 ppbv at lower altitudes. The MLS daily zonal means (thin lines) are averages of approximately 40 individually-retrieved profiles, and the monthly zonal means (thick lines) are averages of approximately 1200 individual profiles. The MLS data are Version 3 which have been multiplied by 0.92, and only data having `QUALITY_CLO` = 4 and `MMAF_STAT=G` have been used. The horizontal extents of the bars give the estimated $\pm 1\sigma$ uncertainty of the SLS measurements and the MLS daily zonal means.

[*Anderson et al.*, 1989, 1991]. Figure 31 compares the 1987 ER-2 measurements with averages from MLS data made inside the vortex during the same time of year and centered at the latitude and longitude of the ER-2 measurements. The dates selected for the comparative MLS measurements were chosen to be within the midrange of corresponding dates for the 1987 ER-2 measurements and when MLS maps showed the edge of enhanced ClO to be at approximately the same location as observed by the ER-2 in 1987. Although there is acceptable agreement at the highest altitudes measured by the ER-2, the problems with MLS Version 3 100-hPa ClO data discussed earlier are evident at the lowest altitudes shown here.

In situ measurements of lower-stratospheric ClO were made [*Avallone et al.*, 1993b; *Toohey et al.*, 1993b] from the ER-2 as part of the Airborne Arctic Stratospheric Expedition II (AASE II) campaign [*Anderson and Toon*, 1993] from September 1991 through March

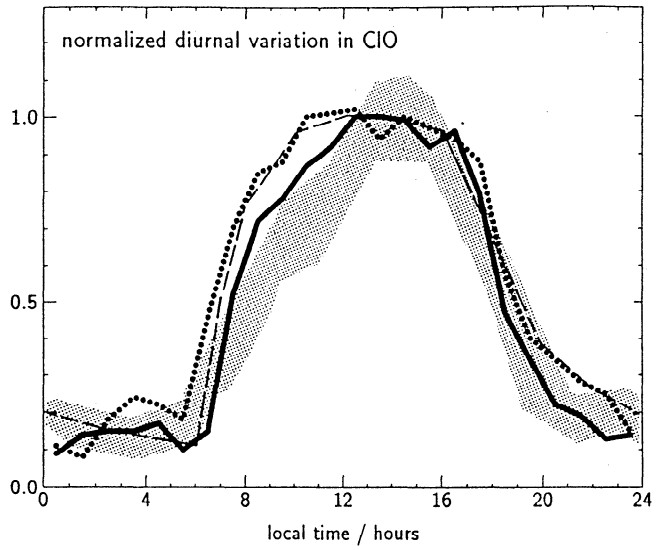

Figure 26. Comparison of diurnal variation in upper stratospheric ClO measured by MLS (solid and dotted lines) and by ground-based techniques (shaded area) [from *Solomon et al.*, 1984]. The model calculation (dashed line) of *Ko and Sze* [1984] as given by *Solomon et al.* [1984] is also shown. The quantity plotted is the column above 30 km for the ground-based measurements and the column above 10 hPa (~31 km) for MLS. The horizontal axis gives local solar time. Both sets of measurements have been normalized to unity peak value, and the 0400 MLS value has been slightly shifted to coincide with the ground-based value. The solid curve is from MLS 10° to 30° N zonal means for December 1991; the dotted curve is from 10° to 30° N zonal means for October 1992. Only MLS data having `MMAF_STAT=G` and `QUALITY_CLO=4` were included. The ground-based results are an average of measurements taken at Hawaii (19° N) during October and December 1982. The MLS measurements (Version 3) have been binned in 1-hour intervals and the horizontal axis gives the local solar time of the measurements (the earlier sunrise and later sunset in October are reflected in the MLS data); between 100 and 500 individually-retrieved profiles were averaged for each local time bin. The ground-based measurements were binned in 2-hour intervals.

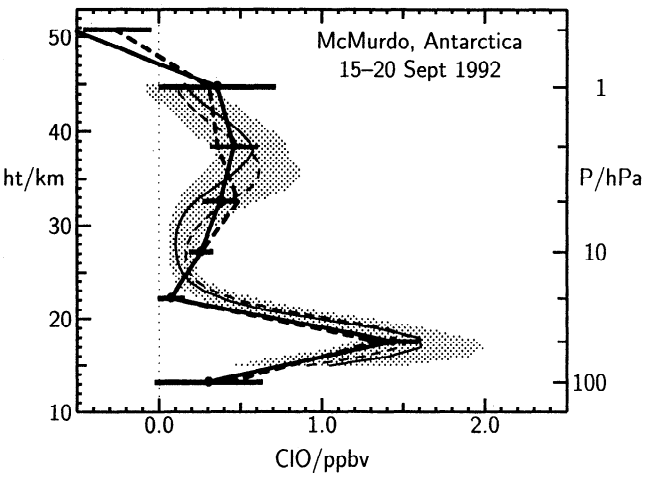

Figure 27. Comparison of ground-based and MLS measurements of the ClO profile over McMurdo Station (78° S, 166°E), Antarctica, during 15–20 September 1992. The thick solid line is the average of all MLS Version 3 profiles at latitudes 75°–80°S and longitudes 140°–190°E (within ~500 km of McMurdo) during 15–20 September 1992, and the results have been multiplied by 0.92. Only data having `MMAF_STAT=G` and `QUALITY_CLO=4` were used. Horizontal bars are the estimated $\pm 1\sigma$ uncertainty in the precision of the MLS averages. The dashed profile is from an iterative retrieval performed after averaging the measured radiances. Heights of the MLS pressure surfaces are from geopotential height obtained from the MLS data. Thin lines show the profiles obtained from the ground-based measurements [*Emmons et al.*, 1995]. The thin solid curve is for measurements on 15 September 1992, and the dashed curve is for measurements on 19–20 September. The shaded area is the $\pm 1\sigma$ total uncertainty (including calibration, atmospheric parameter uncertainties, and retrieval algorithm limitations) estimated by the ground-based team. Day-night differences have been taken at 10 hPa and below for both MLS and ground-based results.

1992, and have precision better than 0.01 ppbv. Monthly zonal means of MLS data are required to reduce its noise to a level at which comparisons with the midlatitude ER-2 data are meaningful. Plate 2 shows height-latitude contour plots of MLS monthly zonal averages to put in context the more detailed midlatitude comparisons with the ER-2 measurements shown below. The increase in lower-stratospheric ClO between October 1991 and March 1992 at ~30°–50°N seen by the ER-2 [*Fahey et al.*, 1993] is evident in these MLS monthly zonal mean data. We also note that the increase in the upper-stratospheric (~2.2–4.6 hPa) ClO from equator to pole seen in the MLS data agrees qualitatively with the predictions of *Solomon and Garcia* [1984]. Smaller abundances of upper-stratospheric ClO are expected at low latitudes where increased CH_4 quenches reactive chlorine, and UARS CLAES measurements [*Kumer et al.*, 1993] show more upper-stratospheric CH_4 at low latitudes, as expected there due to ascending tropical air. Quantitative agreement of theoretical model predictions with MLS upper-stratospheric ClO (and with UARS HALOE HCl) is substantially improved [*Eckman et al.*, 1995] by including 5% branching ratio of the reaction OH+ClO to HCl+O_2. (HCl production from OH+ClO has not been detected in the laboratory, but only an upper limit of 14% has been placed on the branching ratio of OH+ClO to HCl+O_2 [*DeMore et al.*, 1994]. Previously, *Toumi and Bekki* [1993] had found that a 5% branching ratio of OH+ClO

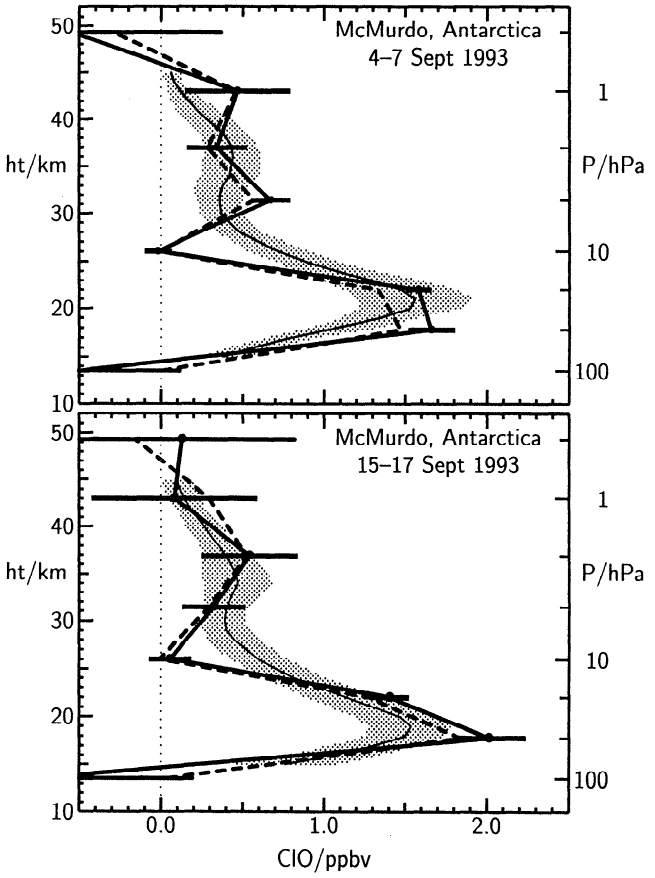

Figure 28. Comparison of ground-based and MLS measurements of the ClO profile over McMurdo Station (78°S, 166°E), Antarctica, during (top) 4–7 September 1993 and (bottom) during 15–17 September 1993. The thick solid lines are the averages of profiles at latitudes 75°–80°S and longitudes 140°–190°E (within ~500 km of McMurdo) from the MLS Version 3 data multiplied by 0.92. The dashed lines are an average of the same MLS observations but from an iterative retrieval performed after averaging the measured radiances. Only MLS data having `MMAF_STAT=G` and `QUALITY_CLO=4` were used. The horizontal range of the bars on MLS profile retrieval points are the estimated uncertainty of the MLS average. The thin line is the profile obtained from the ground-based measurements [*deZafra et al.*, 1995]. The shaded area is the $\pm 1\sigma$ total uncertainty (including calibration, atmospheric parameter uncertainties, and retrieval algorithm limitations) estimated by the ground-based team. Day-night differences have been taken at 10 hPa and below for both MLS and ground-based results.

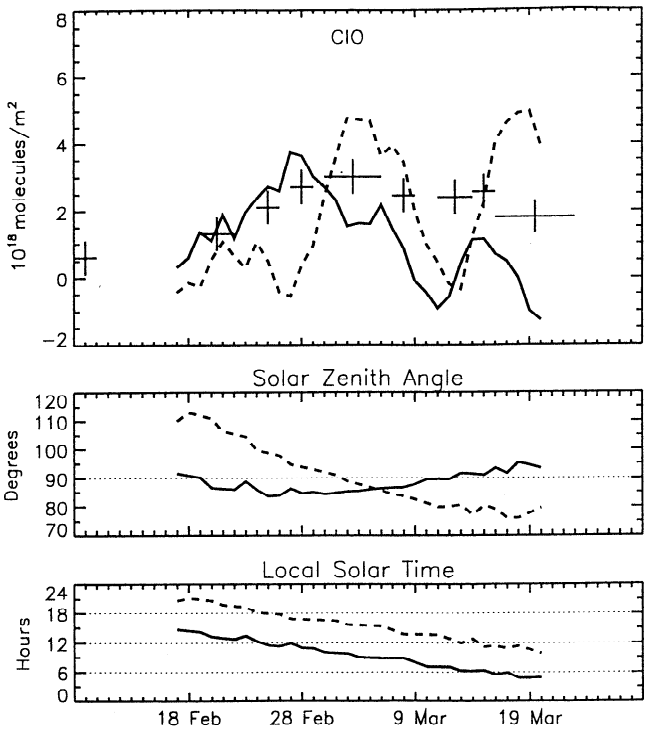

Figure 29. Comparisons of column ClO measurements over Thule, Greenland (76°N, 271°E), in February and March 1992. The pluses are ground-based measurements [*deZafra et al.*, 1994], and the lines are from MLS. The ground-based measurements have been averaged over a period of 3–5 days. The MLS results are a running 5-day smoothing of each day's measurement made nearest Thule; the estimated precision of these smoothed values is $\pm 1 \times 10^{18}$ molecules/m^2. The solid line is for the north-going side of the orbit, the dashed for the south-going side. MLS results are from Version 3 data multiplied by 0.92, and only records having `MMAF_STAT=G` and `QUALITY_CLO=4` have been included. The SZA and local solar time of the MLS measurements are shown in the two bottom panels. Prior to ~9 March only the north-going side of the orbit gave measurements during daylight (when the ground-based measurements were taken) and after ~3 March only the south-going side gave daylight measurements. Thus only the solid curve should be used for comparisons before ~3 March and only the dashed after ~9 March; during ~3–9 March both MLS curves should be comparable to the ground-based measurements. Stratospheric air above Thule was well within the Arctic vortex during late February and up until ~5 March, after which it was near the vortex edge for the period shown here (see discussion in text).

to HCl+O_2 gives better agreement with the upper-stratospheric ClO/HCl ratio measured by SLS [*Stachnik et al.*, 1992]. Figure 32 compares the MLS monthly zonal (day-night) mean measurements, as a function of latitude, with those from the ER-2. The results agree to within the expected MLS precision of ±0.04 ppbv for the monthly zonal mean.

Figure 33 shows ClO versus ozone for ER-2 measurements [*Avallone et al.*, 1993b] made in October 1991 and February 1992, and for MLS monthly zonal (day-night) means from the same time periods and range of latitudes. Despite the very low ClO abundances (relative to MLS individual measurement sensitivity), however, the agreement is within the expected MLS precision.

A time series of MLS 30°–50° N monthly zonal mean lower-stratospheric ClO is shown in Figure 34 and compared with ER-2 and SLS measurements. There is agreement within the estimated MLS precision. Larger abundances of extra-vortical ClO in winter, as shown in these MLS data, are expected due to greater photolysis of HNO_3 in summer (producing more NO_2 which quenches ClO) and, perhaps, to faster rates of certain heterogeneous reactions [*Rodriguez et al.*, 1991;

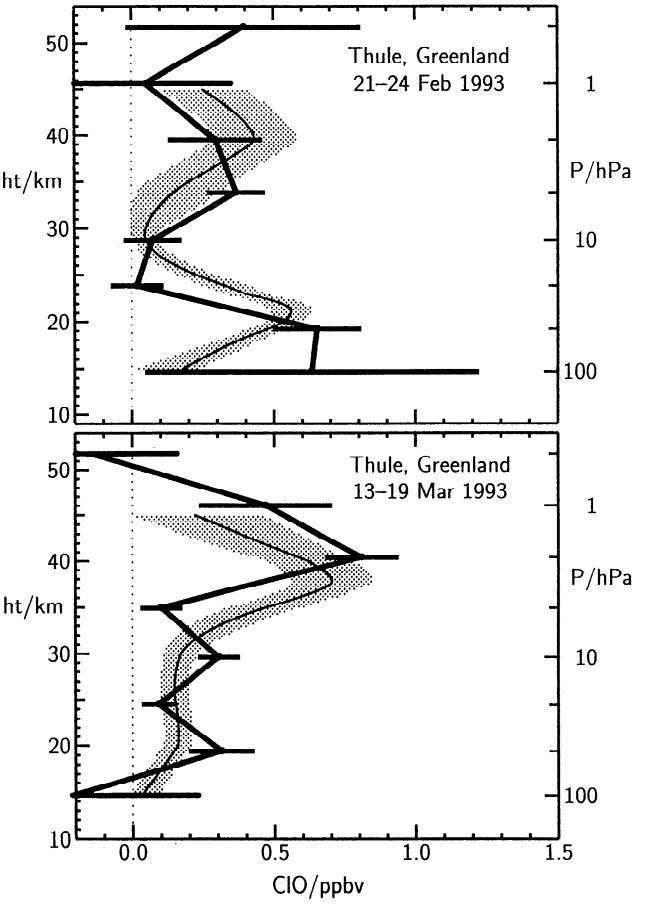

Figure 30. Comparison of ground-based and MLS measurements of the ClO profile over Thule, Greenland, during (top) 21–24 February and (bottom) 13–19 March 1993. The thick solid lines are the averages of profiles at latitudes 73°–79°N and longitudes 271°–311°E (within ~500 km of Thule) from the MLS Version 3 data multiplied by 0.92. Only records having `MMAF_STAT=G` and `QUALITY_CLO=4` were used. The horizontal range of the bars on MLS profile retrieval points are the estimated uncertainty of the MLS average. The thin line is the profile obtained from the ground-based measurements [*Shindell et al.*, 1994]. The shaded area is the $\pm 1\sigma$ uncertainty estimated by the ground-based team. Day-night differences have been taken at 10 hPa and below for both MLS and ground-based results.

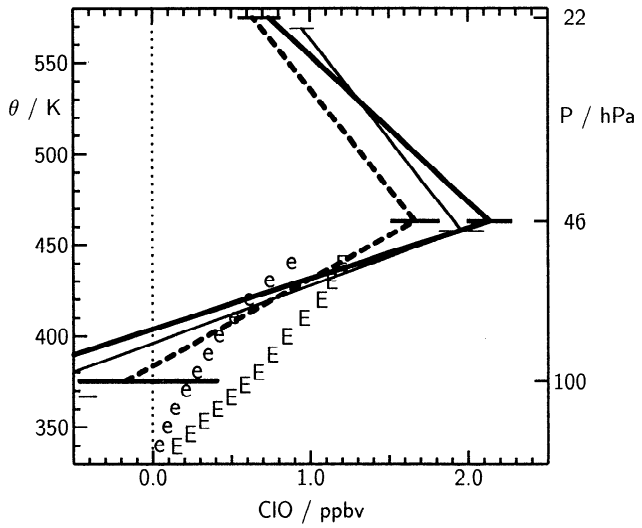

Figure 31. Comparisons of MLS September 1992 and 1993 Antarctic ClO profiles with that measured by the ER-2 aircraft in September 1987. The vertical coordinate indicated on the left is potential temperature, and pressures at MLS retrieval points are indicated on the right. The MLS measurements shown here are averages over 71°–73°S latitude and 0°–140°W longitude, for the periods 6–11 September 1992 (thin lines), and 7–12 September 1993 (thick lines). These periods were chosen to be in the middle of the corresponding 1987 dates of the ER-2 flights and when MLS maps showed the edge of enhanced ClO to be at approximately the same location as seen by the ER-2 in 1987. Solid lines are averages of individual MLS Version 3 profiles multiplied by 0.92; dashed lines are iterative retrievals on averaged radiances from the same data sample. The iterative retrievals use the revised O_2 linewidth for pointing and account for the effects of HNO_3. Day–night differences have been taken for all the MLS data shown here, and horizontal bars give the estimated $\pm 1\sigma$ precision. The ER-2 profiles (e,E) were made at approximately 72° S, 70° W. The lower values (e) are the averages from 10 flights occurring between 23 August and 22 September 1987 reported by *Anderson et al.*, [1989]; the higher values (E) are the ER-2 results after recalibration. The uncertainty in the absolute values of the recalibrated ER-2 data is ±25%, at 90% confidence limits [*Anderson et al.*, 1991].

Solomon et al., 1993; *Tie et al.*, 1994]. This seasonal variation in ClO, which is also observed by MLS in the southern hemisphere (see Figure 4-7 of *Jones et al.* [1995]), can be quantitatively explained by two-dimensional model calculations (e.g., R.S. Harwood, private communication, 1995). The winter seasonal increase in observed midlatitude ClO starts before significant activation of chlorine by polar stratospheric clouds (PSC) in the polar vortex, so it is not likely due to "leakage" of PSC-activated air from the vortex.

Comparisons of MLS ClO results with ER-2 measurements of enhanced lower-stratospheric ClO in the Arctic 1991–1992 winter vortex have been made. All show excellent agreement in the location of enhanced ClO. Figure 35 is a scatterplot of individual MLS ClO measurements versus near-coincident ER-2 measurements and shows agreement to within the MLS noise. Table 4 gives details of the individual measurements which were included in Figure 35.

Figure 36 compares ClO profiles measured on the ER-2 flight into the Arctic vortex on 20 January 1992 [*Toohey et al.*, 1993b], when the largest ClO abundances were measured by the ER-2 during the AASE II campaign, with the average of profiles measured by MLS during 9–11 January 1992 in the vortex region where it observed largest ClO [*Waters et al.*, 1993b]. MLS turned to south-viewing on 14 January 1992, so there are no measurements to compare directly with the 20 January ER-2 results. Even though the measurements compared in Figure 36 were obtained 10 days apart and at different locations in the vortex, there is good agreement between the MLS ClO average profile values and the ER-2 measurements in the upper portion of the ER-2 profile. Problems with the MLS measurements near 100 hPa, as discussed previously, are also evident here.

Comparisons with the SUMAS submillimeter aircraft measurements made in the Arctic vortex in February 1993 [*Crewell et al.*, 1995] also show excellent agreement in location of the enhanced lower-stratospheric ClO. ClO column abundances in conditions of enhanced lower-stratospheric ClO measured by the two techniques agree to ~20% (after corrections identified here have been made to the MLS Version 3 data) with the MLS value being larger; this remaining difference is within the expected uncertainties of the two experiments.

7. Conclusions and Plans for Further Work

Comparisons done to date between MLS and correlative measurements of ClO indicate agreement to within the combined uncertainties of the correlative measurements and the estimated MLS uncertainties given in Table 3 and Figure 21. We believe the MLS ClO data are reliable to within these stated uncertainties. Artifacts in the Version 3 ClO have been identified and are also summarized in Table 3.

MLS ClO data should be used for scientific analyses only when `MMAF_STAT=G`, `QUALITY_CLO=4`, and the estimated uncertainty given in the data files is positive. The quantities `MMAF_STAT` and `QUALITY_CLO` are given, for each retrieved profile, in the companion "paramcter" file accompanying each Level 3 data file.

The ClO data in the MLS Version 3 files can be improved by: (1) multiplying all values by 0.92 to account for inadvertent use of an "old" ClO line strength file in Version 3 processing; (2) averaging individual profiles to reduce the uncertainties due to measurement noise, but remembering that "bias" and "scaling" uncertainties are not reduced by averaging; (3) making ad-

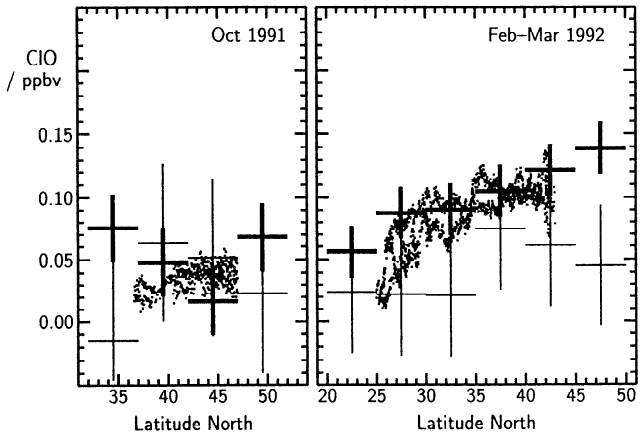

Figure 32. Comparison of ER-2 lower-stratospheric midlatitude ClO measurements with zonal means from MLS. ER-2 values (points) are individual measurements made between 50 and 65 hPa on 4, 6, 10, 12, and 14 October 1991 (left panel) and on 15, 18, 20 and 22 March 1992 (right panel). MLS values (pluses) for 1–31 October 1991 (left panel) and 15 February through 22 March 1992 (right panel) are 5° zonal means with day–night differences taken. The thick pluses are from MLS retrieval values at 46 hPa, and the thin pluses are values at 68 hPa (which are averages of the retrieval values for 46 and 100 hPa); these are Version 3 data multiplied by 0.92. The vertical extents of the pluses are the estimated $\pm 1\sigma$ precision of the MLS zonal means.

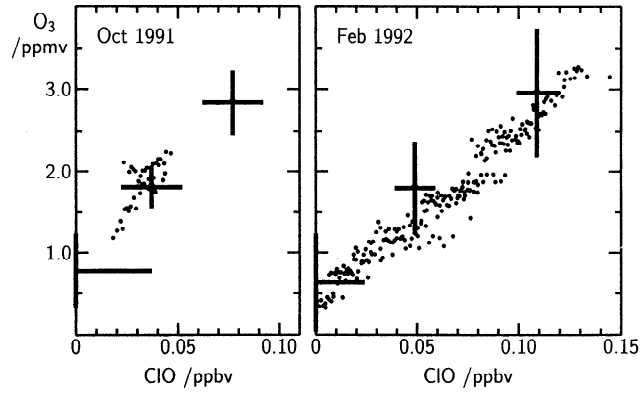

Figure 33. Midlatitude lower-stratospheric ClO versus ozone from ER-2 (points) [*Avallone et al.*, 1993b] and MLS (pluses). The left panel shows measurements made at 40°–60°N on 14 October 1991 by the ER-2 and during 1–31 October 1991 by MLS. The right panel shows measurements made at 20°–50° N on 22 February 1992 by ER-2, and 15 February through 22 March 1992 by MLS. The top pluses are MLS values at 46 hPa, the middle pluses at 68 hPa, and the bottom at 100 hPa. MLS values are monthly zonal means from Version 3, with ClO values multiplied by 0.92 and day-night differences taken. The horizontal extents of the pluses are the observed $\pm 1\sigma$ of individual MLS ClO measurements divided by the square root of the number of measurements (~5000) which were averaged, and gives the estimated precision of the ClO zonal mean. The vertical extents of the pluses are the observed $\pm 1\sigma$ of the individual MLS O_3 measurements. Only MLS data having `MMAF_STAT=G` and `QUALITY_CLO=4` have been included.

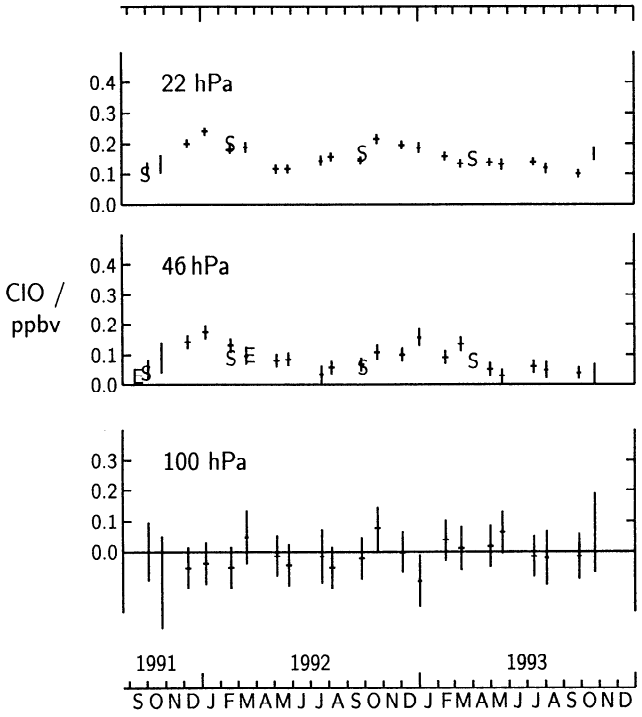

Figure 34. Time series of 30°–50° N monthly zonal means of MLS lower-stratospheric ClO data (pluses, Version 3 data multiplied by 0.92) compared with ER-2 (E) and SLS (S) measurements. MLS data from the night side of the orbit have been subtracted to remove biases. The vertical extents of the pluses give the estimated precision of the MLS means, and the horizontal extents give the time period over which the data were taken. The ER-2 measurements [*Fahey et al.*, 1993] were made at 50-65 hPa.

ditive corrections of +0.1 ppbv at 46 hPa, +0.15 ppbv at 22 hPa, +0.1 ppbv at 10 hPa, and +0.05 ppbv at 4.6 hPa to account for known bias errors in the retrievals; (4) making, when lower-stratospheric HNO_3 is depleted in the polar winter vortices, an additional additive correction of −0.2 ppbv at 22 and 46 hPa to account for the effects of HNO_3 on the ClO retrievals; (4) making, when temperatures are below 195 K, an additional 0.92 multiplication to 22- and/or 46-hPa ClO values in the polar winter vortex regions to account for limitations of the Version 3 algorithms (the value of 0.92 used here is a typical correction factor determined from results using iterative retrieval algorithms on various polar vortex situations as described in this paper; a more accurate correction of Version 3 data for any particular situation requires detailed analyses of that situation; after this correction is applied we would expect the scaling uncertainty at 22 and 46 hPa to be reduced from 15% to ~10%); (6) taking day-night differences, when possible, to reduce bias errors.

At least two future reprocessings of MLS data are planned. The first is principally aimed at producing a lower-stratospheric HNO_3 data set from MLS, which was not done for Version 3. This reprocessing will also

Table 4. Individual MLS ClO Measurements and Near-Coincident ER-2 Measurements in the 1991–1992 Arctic Winter Vortex

	ER-2					MLS							
1992	UT	Lat °N	Long °W	θ, K	ClO, ppbv	UT	Lat °N	Long °W	Rec. Num.	SZA, deg	LST, hour	ClO at 46 hPa, ppbv	ClO at θ, ppbv
4 Jan.	1805	58	56	475	0.5±0.3	1716	57	48	949	84.1	14.0	0.4±0.4	0.6±0.4
	1930	51	63	490	0.1±0.02	1855	51	67	1039	79.8	14.3	0.2±0.4	0.0±0.4
						1856	47	65	1040	87.7	14.5	−0.2±0.4	0.2±0.4
6 Jan.	1600	61	44	450	0.8±0.1	1543	65	42	864	87.8	12.8	1.0±0.4	0.8±0.4
						1544	62	38	865	85.0	13.1	1.5±0.4	0.9±0.4
	1830	55	56	475	0.12±0.03	1722	55	57	955	79.6	13.5	0.2±0.4	0.2±0.4
8 Jan.	1615	61	44	450	0.4±0.2	1549	62	50	869	84.4	12.4	1.6±0.4	0.6±0.4
						1550	59	47	870	81.3	12.6	0.6±0.4	0.4±0.4
	1410	51	63	465	0.35±0.25	1728	52	66	960	75.3	12.9	0.2±0.4	0.3±0.4
	1930	49	65	500	0.14±0.03	1729	49	64	961	72.3	13.1	0.6±0.4	0.4±0.4
17 Feb.	1720	68	61	450	0.6±0.2	1730	68	62	961	81.0	13.1	0.5±0.4	0.4±0.4
						1554	68	37	873	81.3	13.2	−0.3±0.4	0.7±0.4
	1755	65	63	480	0.75±0.1	1729	65	66	960	77.4	12.8	0.2±0.4	0.5±0.4
						1553	65	42	872	77.6	12.9	0.9±0.4	0.6±0.4
	1830	61	65	485	0.7±0.1	1728	61	70	959	73.8	12.6	0.6±0.4	0.6±0.4
						1552	62	45	871	74.0	12.6	−0.1±0.4	0.2±0.4
	1900	58	66	495	0.3±0.1	1727	58	73	958	70.2	12.4	0.6±0.4	0.6±0.4
						1551	58	48	870	70.5	12.4	0.1±0.4	0.2±0.4
	1930	55	67	510	0.17±0.06	1726	55	75	957	66.7	12.2	0.6±0.4	0.4±0.4
						1550	55	51	869	66.9	12.2	0.3±0.4	0.3±0.4
	2020	51	67	500	0.10±0.02	1725	51	78	956	63.2	12.0	0.4±0.4	0.1±0.4
						1549	51	53	868	63.5	12.0	0.3±0.4	0.2±0.4

Universal time (UT), latitude, longitude, and potential temperature (θ) of the ER-2 measurements are indicated. The range of ClO values shown here for the ER-2 measurements is the range of values which were measured over a spatial region of the approximate size as that sampled during individual MLS measurements. Also given for the MLS measurements are the record number (in the daily MLS data file), SZA, and the local solar time (LST) of the measurements. The MLS data are Version 3 multiplied by 0.92, and values are given for the 46-hPa retrieval point and from the retrieved vertical profile interpolated to the potential temperature of the corresponding ER-2 measurement.

correct the 8% scaling error in Version 3 due to inadvertent use of the old line strength file, use the retrieved HNO_3 to account for its effects on ClO, use tangent pressure retrieved with the revised O_2 linewidth parameter, and use better "space radiances" (from improved Level 1 processing) which should improve ClO retrievals above 1 hPa. A later reprocessing, aimed principally at producing an upper tropospheric H_2O data set from MLS, will also use iterative algorithms to eliminate limitations caused by the linearized Version 3 algorithms.

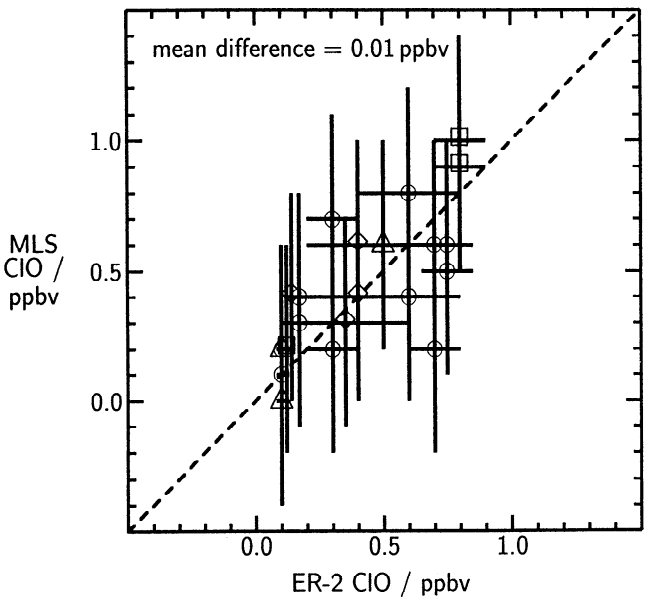

Figure 35. Scatterplot of individual MLS ClO measurements versus near-coincident ER-2 measurements. The ER-2 measurements [*Toohey et al.*, 1993b] were made during flights north from Bangor, Maine, as part of the AASE II campaign. The MLS values (Version 3 data, multiplied by 0.92) are taken from MLS vertical profiles at the potential temperature of the ER-2 measurement. Numerical values, locations and times of the measurements are given in Table 4. Symbols indicate measurements on 4 January (triangles), 6 January (squares), 8 January (diamonds), and 17 February (circles) 1992. The vertical extent of each plus is the $\pm 1\sigma$ MLS measurement noise, and the horizontal extent indicates the range of values measured by the ER-2 over the approximate spatial area sampled by MLS. The diagonal dashed line is where points would lie if there were perfect agreement. The mean difference of 0.01 ppbv is the average value of the difference (MLS ER2) in all measurements shown here; the standard deviation of the individual differences is 0.2 ppbv.

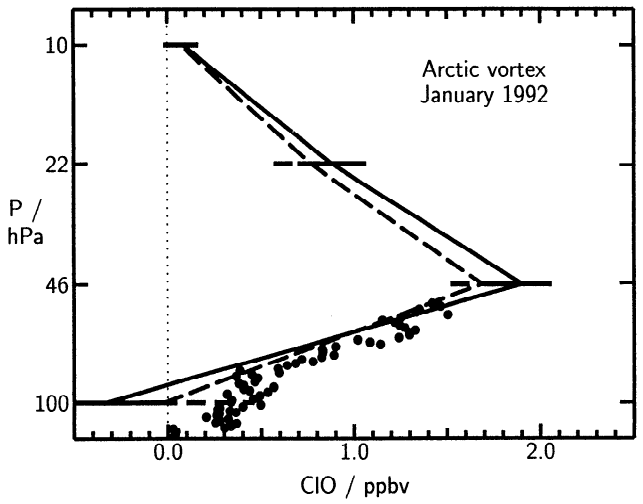

Figure 36. Comparison of largest ClO abundances from MLS (solid and dashed lines) and ER-2 (points) measured in the Arctic vortex during January 1992. The MLS profiles are the average of all measurements made during 9–11 January between 55°–65°N and 0°–60°E (see Figure 4 of *Waters et al.* [1993b]). The solid line is from the Version 3 data multiplied by 0.92, as discussed in the text; the dashed line is from an improved iterative retrieval algorithm. The ER-2 measurements [*Toohey et al.*, 1993b] are a combination of two profiles measured within the vortex on 20 January: one at 68°N, 60°W, measured at local times within one-half hour of noon, and the other at 54°N, 67°W, measured between 1330 and 1415 Local Times. The MLS measurements are averages of day-night differences, and only data having `MMAF_STAT=G` and `QUALITY_CLO=4` are included. The MLS day measurements were at local solar times within 1 hour of noon (SZA of 77°–86°); the night measurements were at local solar times between midnight and 0200. The horizontal extent of each bar gives the estimated $\pm 1\sigma$ precision for the MLS day-night average. Systematic uncertainties for the MLS measurements are discussed in the text. Uncertainty in the absolute values of the ER-2 measurements is $\pm 15\%$ ($\pm 2\sigma$).

Acknowledgments. This paper is dedicated to the memory of our colleague C.C. Voge who managed MLS software development for many years. We thank J.R. Holden, R.R. Lay, and M.S. Loo for their contributions to prelaunch testing and in-orbit operations; F.T. Barath for management of MLS during its development phase and G.K. Lau for management during its operational phase; and our colleagues on the engineering team which developed the instrument. We thank E.A. Cohen and J.J. Oh for measuring the oxygen broadening of the MLS ClO spectral line so quickly after our measurements suggested the need for it, and G.L. Manney, T. Luu, and R.W. Zurek for providing derived meteorological quantities used operationally on a daily basis in checking the "reasonableness" of enhanced ClO distributions observed by MLS. We are grateful to W.G. Grose and his UARS team for atmospheric model data used in prelaunch testing; to D.J. Wuebbles and his UARS team for model ClO data used as "climatology," and to R. Seals and colleagues for assembling a "climatology" for use in UARS data processing. We thank H.M. Pickett, M.R. Schoeberl, A.R. Douglass, L.S. Elson, M.L. Santee, G.L. Manney, R.S. Harwood, W.A. Lahoz, G.E. Peckham, C.D. Rodgers and B.J. Connor for helpful discussions. Finally, we thank all our UARS colleagues, especially those responsible for the UARS Central Data Handling Facility, for their support and encouragement throughout many years of working together. The research performed at the Jet Propulsion Laboratory, California Institute of Technology, was under contract with the U.S. National Aeronautics and Space Administration and sponsored through its UARS project.

References

Aellig, C. P., N. Kampfer, and R. M. Bevilacqua, Error analysis of ClO, O_3, and H_2O abundance profiles retrieved from millimeter wave limb sounding measurements, *J. Geophys. Res.*, *98*, 2975–2983, 1993.

Anderson, J. G., and O. B. Toon, Airborne Arctic Stratospheric Expedition II: An overview, *Geophys. Res. Lett.*, *20*, 2499–2502, 1993.

Anderson, J. G., J. J. Margitan, and D. H. Stedman, Atomic chlorine and the chlorine monoxide radical in the stratosphere: Three in situ observations, *Science*, *198*, 501–503, 1977.

Anderson, J. G., W. H. Brune, and M. H. Proffitt, Ozone destruction by chlorine radicals within the Antarctic vortex: The spatial and temporal evolution of ClO–O_3 anticorrelation based on in situ ER-2 data, *J. Geophys. Res.*, *94*, 11,465–11,479, 1989.

Anderson, J. G., D. W. Toohey, and W. H. Brune, Free radicals within the Antarctic vortex: The role of CFCs in Antarctic ozone loss, *Science*, *251*, 39–46, 1991.

Avallone, L. M., D. W. Toohey, W. H. Brune, R. J. Salawitch, A. E. Dessler, and J. G. Anderson, Balloon-borne in situ measurements of ClO and ozone: Implications for heterogeneous chemistry and mid-latitude ozone loss, *Geophys. Res. Lett.*, *20*, 1795–1798, 1993a.

Avallone, L. M., D. W. Toohey, M. H. Proffitt, J. J. Margitan, K. R. Chan, and J. G. Anderson, In-situ measurements of ClO at mid-latitudes: Is there an effect from Mt. Pinatubo?, *Geophys. Res. Lett.*, *20*, 2519–2522, 1993b.

Barath, F. T., et al., The Upper Atmosphere Research Satellite Microwave Limb Sounder Instrument, *J. Geophys. Res.*, *98*, 10,751–10,762, 1993.

Barrett, J. W., P. M. Solomon, R. L. deZafra, M. Jaramillo, L. Emmons, and A. Parrish, Formation of the Antarctic ozone hole by the ClO dimer mechanism, *Nature*, *336*, 455–458, 1988.

Bell, W., N. A. Martin, T. D. Gardiner, N. R. Swann, P. T. Woods, P. F. Fogal, and J. W. Waters, Column measurements of stratospheric trace species over Åre, Sweden in the winter of 1991-92, *Geophys. Res. Lett.*, *21*, 1347–1350, 1994.

Brune, W. H., E. M. Weinstock, M. J. Schwab, R. M. Stimpfle, and J. G. Anderson, Stratospheric ClO: In-situ detection with a new approach, *Geophys. Res. Lett.*, *12*, 441–444, 1985.

Brune, W. H., E. M. Weinstock, and J. G. Anderson, Midlatitude ClO below 22 km altitude: Measurements with a new aircraft-borne instrument, *Geophys. Res. Lett.*, *15*, 144–147, 1988.

Carli, B., F. Mencaraglia, M. Carlotti, B. M. Dinelli, and I. Nolt, Submillimeter measurement of stratosphric chlorine monoxide, *J. Geophys. Res.*, *93*, 7063–7068, 1988.

Chance, K. V., D. G. Johnson, W. A. Traub, and K. W. Jucks, Measurements of the stratospheric hydrogen peroxide profile using far infrared thermal emission spectroscopy, *Geophys. Res. Lett.*, *18*, 1003–1006, 1991.

Craig, H., Isotopic standards for carbon and oxygen and correction factors for mass-spectrometric analysis of carbon dioxide, *Geochim. Cosmochim. Acta.*, *12*, 133–149, 1957.

Crewell, S., K. Künzi, H. Nett, T. Wehr, and P. Hartogh, Aircraft measurements of ClO and HCl during EASOE 1991/92, *Geophys. Res. Lett.*, *21*, 1267–1270, 1994.

Crewell, S., R. Fabian, K. Künzi, H. Nett, T. Wehr, W. Read, and J. Waters, Comparison of ClO measurements made by airborne and spaceborne microwave radiometers in the Arctic winter stratosphere 1993, *Geophys. Res. Lett.*, *22*, 1489–1492, 1995.

DeMore, W. B., S. P. Sander, D. M. Golden, R. F. Hampson, M. J. Kurylo, C. J. Howard, A. R. Ravishankara, C. E. Kolb, and M. J. Molina, Chemical kinetics and photochemical data for use in stratospheric modeling: Evaluation number 10, *Tech. Rep. 94-26*, Jet Prop. Lab., Pasadena, Calif., 1994.

Dessler, A. E., et al., Correlated observations of HCl and $ClONO_2$ from UARS and implications for stratospheric chlorine partitioning, *Geophys. Res. Lett.*, *22*, 1721–1724, 1995.

deZafra, R. L., M. Jaramillo, A. Parrish, P. Solomon, B. Connor, and J. Barrett, High concentrations of chlorine monoxide at low altitudes in the Antartic spring stratosphere: Diurnal variation, *Nature*, *328*, 408–411, 1987.

deZafra, R. L., M. Jaramillo, J. Barrett, L. K. Emmons, P. Solomon, and A. Parrish, New observations of a large concentration of ClO in the springtime lower stratosphere over Antarctica and its implications for ozone-depleting chemistry, *J. Geophys. Res.*, *94*, 11,423–11,428, 1989.

deZafra, R. L., L. K. Emmons, J. M. Reeves, and D. T. Shindell, An overview of millimeter-wave spectroscopic measurements of chlorine monoxide at Thule, Greenland, February–March, 1992: Vertical profiles, diurnal variation and longer-term trends, *Geophys. Res. Lett.*, *21*, 1271–1274, 1994.

deZafra, R. L., J. M. Reeves, and D. T. Shindell, Chlorine monoxide in the Antarctic spring vortex 1: Evolution of midday vertical profiles over McMurdo Station, 1993, *J. Geophys. Res.*, *100*, 13,999–14,007, 1995.

Douglass, A., et al., A 3D simulation of the early winter distribution of reactive chlorine in the north polar vortex, *Geophys. Res. Lett.*, *20*, 1271–1274, 1993.

Douglass, A. R., M. R. Schoeberl, R. S. Stolarski, J. W. Waters, J. M. Russell III, and A. E. Roche, Interhemispheric differences in springtime production of HCl and $ClONO_2$ in the polar vortices, *J. Geophys. Res.*, *100*, 13,967–13,978, 1995.

Eckman, R. S., W. L. Grose, R. E. Turner, W. T. Blackshear, J. M. Russell III, L. Froidevaux, J. W. Waters, J. B. Kumer, and A. E. Roche, Stratospheric trace constituents simulated by a three-dimensional general circulation model: Comparison with UARS data, *J. Geophys. Res.*, *100*, 13,951–13,966, 1995.

Elson, L. S., and L. Froidevaux, The use of Fourier transforms for asynoptic mapping: Early results from the Upper Atmosphere Research Satellite Microwave Limb Sounder, *J. Geophys. Res.*, *98*, 23,039–23,049, 1993.

Emmons, L. K., J. M. Reeves, D. T. Shindell, and R. L. deZafra, N_2O as an indicator of Arctic vortex dynamics: Correlations with O_3 over Thule, Greenland in February and March, 1992, *Geophys. Res. Lett.*, *21*, 1275–1278, 1994.

Emmons, L. K., D. T. Shindell, J. M. Reeves, and R. L. deZafra, Stratospheric ClO profiles from McMurdo Station, Antarctica, spring 1992, *J. Geophys. Res.*, *100*, 3049–3055, 1995.

Fahey, D. W., et al., *In situ* measurements constraining the role of sulphate aerosols in mid-latitude ozone depletions, *Nature*, *363*, 509–514, 1993.

Fahey, D. W., et al., Polar Ozone, in *Scientific Assessment of Stratospheric Ozone, 1994*, chap. 3. World Meteorological Organization and United Nations Environment Program, 1995.

Farman, J. C., B. G. Gardiner, and J. D. Shanklin, Large losses of total ozone in Antarctica reveal seasonal ClO_x/NO_x interaction, *Nature*, *315*, 207–210, 1985.

Fishbein, E. F., et al., Validation of UARS Microwave Limb Sounder temperature and pressure measurements, *J. Geophys. Res.*, this issue.

Froidevaux, L., et al., Validation of UARS Microwave Limb Sounder ozone measurements, *J. Geophys. Res.*, this issue.

Geller, M. A., Y. Chi, R. B. Rood, A. R. Douglass, D. J. Allen, M. Cerniglia, and J. W. Waters, 3-D transport-chemistry studies of the stratosphere using satellite data together with data assimilation, in *The Role of the Stratosphere in Global Change*, edited by M.-L. Chanin. Springler-Verlag, New York, 1993.

Gille, J. C., P. L. Bailey, and C. A. Craig, Revised reference model for nitric acid, in *Middle Atmosphere Program Handbook for MAP vol. 31*, edited by G. M. Keating, chap. 6. ICSU Sci. Comm. on Sol. Terr. Phys. (SCOSTEP), Univ. of Ill., Urbana, 1989.

Grose, W. L., and J. C. Gille, Upper Atmosphere Research

Satellite validation workshop III report: Temperature and constituents validation, *NASA Conference Publication CP-3317*, 1996.

Gunson, M. R., M. C. Abrams, L. L. Lowes, E. Mahieu, R. Zander, C. P. Rinsland, M K W Ko, N. D. Sze, and D. K. Weisenstein, Increase in levels of stratospheric chlorine and fluorine loading between 1985 and 1992, *Geophys. Res. Lett.*, *21*, 2223–2226, 1994.

Janssen, M. A. (Ed.), *Atmospheric Remote Sensing by Microwave Radiometry*. John Wiley, New York, 1993.

Jarnot, R. F., R. E. Cofield, J. W. Waters, G. E. Peckham, and D. A. Flower, Calibration of the Microwave Limb Sounder on the Upper Atmosphere Research Satellite, *J. Geophys. Res.*, this issue.

Jones, R. L., et al., Tropical and midlatitude ozone, in *Scientific Assessment of Stratospheric Ozone, 1994*, chap. 4. World Meteor. Organ. U.N. Environ. Program, Geneva, 1995.

Ko, M. K. W., and N. D. Sze, Diurnal variation of ClO: Implications for the stratospheric chemistries of $ClONO_2$, HOCl, and HCl, *J. Geophys. Res.*, *89*, 11,619–11,632, 1984.

Kumer, J. B., J. L. Mergenthaler, and A. E. Roche, CLAES CH_4, N_2O and CCl_2F_2 global data, *Geophys. Res. Lett.*, *20*, 1239–1242, 1993.

Lahoz, W. A., et al., Validation of UARS Microwave Limb Sounder 183 GHz H_2O measurements, *J. Geophys. Res.*, this issue.

Liebe, H. J., G. A. Hufford, and R. O. DeBolt, The atmospheric 60-GHz oxygen spectrum: Modeling and laboratory measurements, *Tech. Rep. NTIA 91-272*, Nat. Telecommun. and Inf. Admin., Inst. for Telecommun. Sci., Boulder, Colo., 1991a.

Liebe, H. J., G. A. Hufford, and R. O. DeBolt, Measurements of the 60 GHz O_2 spectrum of air, in *URSI Radio Science Meeting, Union Radio Sci. Int., London, Ontario, Canada.* 1991b.

Liebe, H. J., P. W. Rosenkranz, and G. A. Hufford, Atmospheric 60 GHz oxygen spectrum: New laboratory measurements and line parameters, *J. Quant. Spectrosc. Radiat. Transfer*, *48*, 629–643, 1992.

Manney, G. L., L. Froidevaux, J. W. Waters, L. S. Elson, E. F. Fishbein, R. W. Zurek, R. S. Harwood, and W. A. Lahoz, The evolution of ozone observed by UARS MLS in the 1992 late winter southern polar vortex, *Geophys. Res. Lett.*, *20*, 1279–1282, 1993.

Manney, G. L., et al., Chemical depletion of ozone in the Arctic lower stratosphere during winter 1992-93, *Nature*, *370*, 429–434, 1994.

Manney, G. L., R. W. Zurek, L. Froidevaux, and J. W. Waters, Evidence for arctic ozone depletion in late February and early March 1994, *Geophys. Res. Lett.*, *22*, 2941–2944, 1995a.

Manney, G. L., L. Froidevaux, J. W. Waters, and R. W. Zurek, Evolution of microwave limb sounder ozone and the polar vortex during winter, *J. Geophys. Res.*, *100*, 2953–2972, 1995b.

Marks, C. J., and C. D. Rodgers, A retrieval method for atmospheric composition from limb emission measurements, *J. Geophys. Res.*, *98*, 14,939–14,953, 1993.

Mauersberger, K., Ozone isotope measurements in the stratosphere, *Geophys. Res. Lett.*, *14*, 80–83, 1987.

Menzies, R. T., Remote measurement of ClO in the stratosphere, *Geophys. Res. Lett.*, *6*, 151–154, 1979.

Menzies, R. T., A re-evaluation of laser heterodyne radiometer ClO measurements, *Geophys. Res. Lett.*, *10*, 729–732, 1983.

Molina, L. T., and M. J. Molina, Production of Cl_2O_2 from the self-reaction of the ClO radical, *J. Phys. Chem.*, *91*, 433–436, 1987.

Molina, M. J., and F. S. Rowland, Stratospheric sink for chlorofluoromethanes: Chlorine atom catalysed destruction of ozone, *Nature*, *249*, 810–812, 1974.

Nickolaisen, S. L., R. R. Friedl, and S. P. Sander, Kinetics and mechanism of the ClO + ClO reaction: Pressure and temperature dependences of the bimolecular and termolecular channels and thermal decomposition of chlorine peroxide, *J. Phys. Chem.*, *98*, 155–169, 1994.

Njoku, E. G., Passive microwave remote sensing of the Earth from space — A review, *Proc. IEEE*, *79*, 728–750, 1982.

Oh, J. J., and E. A. Cohen, Pressure broadening of ClO by N_2 and O_2 near 204 and 649 GHz and new frequency measurements between 632 and 725 GHz, *J. Quant. Spectrosc. Radiat. Transfer*, *54*, 151–156, 1994.

Parrish, A., R. L. deZafra, P. M. Solomon, J. W. Barrett, and E. R. Carlson, Chlorine oxide in the stratospheric ozone layer: Ground-based detection and measurement, *Science*, *211*, 1158–1161, 1981.

Pickett, H. M., D. E. Brinza, and E. A. Cohen, Pressure broadening of ClO by nitrogen, *J. Geophys. Res.*, *86*, 7279–7282, 1981.

Pickett, H. M., R. L. Poynter, and E. A. Cohen, Submillimeter, millimeter and microwave spectral line catalog, *Tech. Rep. 80-23, rev. 3*, Jet Prop. Lab., Pasadena, Calif., 1992.

Poynter, R. L., and H. M. Pickett, Submillimeter, millimeter and microwave spectral line catalog, *Appl. Opt.*, *24*, 2235–2240, 1985.

Pyle, J. A., et al., An overview of the EASOE campaign, *Geophys. Res. Lett.*, *21*, 1191–1194, 1994.

Read, W. G., L. Froidevaux, and J. W. Waters, Microwave Limb Sounder (MLS) measurements of SO_2 from Mt. Pinatubo volcano, *Geophys. Res. Lett.*, *20*, 1299–1302, 1993.

Read, W. G., J. W. Waters, L. Froidevaux, D. A. Flower, R. F. Jarnot, D. L. Hartmann, R. S. Harwood, and R. B. Rood, Upper-tropospheric water vapor from UARS MLS, *Bull. Am. Meteorol. Soc.*, *76*, 2381–2389, 1995.

Ricaud, P. D., et al., Polar stratospheric clouds as deduced from MLS and CLAES measurements, *Geophys. Res. Lett.*, *22*, 2033–2036, 1995.

Rodgers, C. D., Retrieval of atmospheric temperature and composition from remote measurements of thermal radiation, *Rev. Geophys. and Space Phys.*, *14*, 609–624, 1976.

Rodgers, C. D., Characterization and error analyses of profiles retrieved from remote sounding measurements, *J. Geophys. Res.*, *95*, 5587–5595, 1990.

Rodriguez, J. M., M. K. W. Ko, and N. D. Sze, Role of heterogeneous conversion of N_2O_5 on sulfate aerosols in global ozone losses, *Nature*, *352*, 134–137, 1991.

Santee, M. L., W. G. Read, J. W. Waters, L. Froidevaux, G. L. Manney, D. A. Flower, R. F. Jarnot, R. S. Harwood, and G. E. Peckham, Interhemispheric differences in polar stratospheric HNO_3, H_2O, ClO and O_3, *Science*, *267*, 849–852, 1995.

Schoeberl, M. R., R. S. Stolarski, A. R. Douglass, P. A. Newman, L. R. Lait, J. W. Waters, L. Froidevaux, and W. G. Read, MLS ClO observations and arctic polar vortex temperatures, *Geophys. Res. Lett.*, *20*, 2861–2864, 1993.

Shields, W. R., T. J. Murphy, E. L. Garner, and V. H. Dibeler, Absolute isotopic abundance ratio and the atomic weight of chlorine, *J. Am. Chem. Soc.*, *84*, 1519–1522, 1962.

Shindell, D. T., J. M. Reeves, L. K. Emmons, and R. L. deZafra, Arctic chlorine monoxide observations during spring 1993 over Thule, Greenland, and implications for ozone depletion, *J. Geophys. Res.*, *99*, 25,697–25,704, 1994.

Solomon, P. M., R. deZafra, A. Parrish, and J. W. Barrett, Diurnal variation of chlorine monoxide: A critical test of

chlorine chemistry in the ozone layer, *Science*, *224*, 1210–1214, 1984.

Solomon, P. M., B. Conner, R. L. deZafra, A. Parrish, J. Barrett, and M. Jaramillo, High concentrations of chlorine monoxide at low altitudes in the Antartic spring stratosphere, *Nature*, *328*, 411–413, 1987.

Solomon, S., Progress towards a quantitative understanding of Antarctic ozone depletion, *Nature*, *347*, 347–354, 1990.

Solomon, S., and R. R. Garcia, On the distributions of long-lived tracers and chlorine species in the middle atmosphere, *J. Geophys. Res.*, *89*, 11,633–11,644, 1984.

Solomon, S., R. W. Sanders, R. R. Garcia, and J. G. Keys, Increased chlorine dioxide over Antarctica caused by volcanic aerosols from Mount Pinatubo, *Nature*, *363*, 245–248, 1993.

Stachnik, R. A., J. C. Hardy, J. A. Tarsala, J. W. Waters, and N. R. Erickson, Submillimeterwave heterodyne measurements of stratospheric ClO, HCl, O_3, and HO_2: First results, *Geophys. Res. Lett.*, *19*, 1931–1934, 1992.

Staelin, D. H., Passive remote sensing at microwave wavelengths, *Proc. IEEE*, *57*, 427–439, 1969.

Taylor, F. W., A. Dudhia, and C. D. Rodgers, Proposed reference models for nitrous oxide and methane in the middle atmosphere, in *Middle Atmosphere Program Handbook for MAP, vol. 31*, edited by G. M. Keating, chap. 4. ICSU Sci. Comm. on Sol. Terr. Phy. (SCOSTEP), Univ. of Ill., Urbana, 1989.

Tie, X., G. P. Brasseur, B. Briegleb, and C. Granier, Two-dimensional simulation of Pinatubo aerosol and its effect on stratospheric ozone, *J. Geophys. Res.*, *99*, 20,545–20,562, 1994.

Toohey, D. W., L. M. Avallone, N. T. Allen, J. N. Demusz, J. N. Hazen, and J. G. Anderson, The performance of a new instrument for in situ measurements of ClO in the lower stratosphere, *Geophys. Res. Lett.*, *20*, 1791–1794, 1993a.

Toohey, D. W., L. M. Avallone, L. R. Lait, P. A. Newman, M. R. Schoeberl, D. W. Fahey, E. L. Woodbridge, and J. G. Anderson, The seasonal evolution of reactive chlorine in the northern hemisphere stratosphere, *Science*, *261*, 1134–1136, 1993b.

Toumi, R., and S. Bekki, The importance of the reactions between OH and ClO for stratospheric ozone, *Geophys. Res. Lett.*, *20*, 2447–2450, 1993.

Ulaby, F. T., R. K. Moore, and A. K. Fung, *Microwave Remote Sensing Active and Passive, vol. I, Microwave Remote Sensing Fundamentals and Radiometry.* Addison-Wesley, Reading, Mass., 1981.

Ulaby, F. T., R. K. Moore, and A. K. Fung, *Microwave Remote Sensing Active and Passive, vol. III, From Theory to Applications.* Addison-Wesley, Reading, Mass., 1986.

Waters, J. W., Microwave limb-sounding of Earth's upper atmosphere, *Atmos. Res.*, *23*, 391–410, 1989.

Waters, J. W., Submillimeter heterodyne spectroscopy and remote sensing of the upper atmosphere, *IEEE Proc.*, *80*, 1679–1701, 1992.

Waters, J. W., Microwave Limb Sounding, in *Atmospheric Remote Sensing by Microwave Radiometry*, edited by M. A. Janssen, chap. 8. John Wiley, New York, 1993.

Waters, J. W., J. J. Gustincic, R. K. Kakar, H. K. Roscoe, P. N. Swanson, T. G. Phillips, T. DeGraauw, A. R. Kerr, and R. J. Mattauch, Aircraft search for millimeter wavelength emission by stratospheric ClO, *J. Geophys. Res.*, *84*, 6934, 1979.

Waters, J. W., J. C. Hardy, R. F. Jarnot, and H. M. Pickett, Chlorine monoxide radical, ozone, and hydrogen peroxide: Stratospheric measurements by microwave limb sounding, *Science*, *214*, 61–64, 1981.

Waters, J. W., R. A. Stachnik, J. C. Hardy, and R. F. Jarnot, ClO and O_3 stratospheric profiles: Balloon microwave measurements, *Geophys. Res. Lett.*, *15*, 780–783, 1988.

Waters, J. W., L. Froidevaux, G. L. Manney, W. G. Read, and L. S. Elson, Lower stratospheric ClO and O_3 in the 1992 southern hemisphere winter, *Geophys. Res. Lett.*, *20*, 1219–1222, 1993a.

Waters, J. W., L. Froidevaux, W. G. Read, G. L. Manney, L. S. Elson, D. A. Flower, R. F. Jarnot, and R. S. Harwood, Stratospheric ClO and ozone from the Microwave Limb Sounder on the Upper Atmosphere Research Satellite, *Nature*, *362*, 597–602, 1993b.

Waters, J. W., G. L. Manney, W. G. Read, L. Froidevaux, D. A. Flower, and R. F. Jarnot, UARS MLS observations of lower stratospheric ClO in the 1992–93 and 1993–94 arctic winter vortices, *Geophys. Res. Lett.*, *22*, 823–826, 1995.

Weinstock, E. M., M. J. Phillips, and J. G. Anderson, In situ observations of ClO in the stratosphere: A review of recent results, *J. Geophys. Res.*, *86*, 7273–7278, 1981.

Wofsy, S. C., Temporal and latitudinal variations of stratospheric trace gases: A critical comparison between theory and experiment, *J. Geophys. Res.*, *83*, 364–378, 1978.

Yaron, D., K. Peterson, and W. Klemperer, On the dipole moment functions of ClO and OH, *J. Chem. Phys.*, *88*, 4702–4710, 1988.

L.M. Avallone and D.W. Toohey, Earth System Science Department, University of California at Irvine, Irvine, CA 92717.

J.R. Burke, R.E. Cofield, E.F. Fishbein, D.A. Flower, L. Froidevaux, J.C. Hardy, R.F. Jarnot, T.A. Lungu, L.L. Nakamura, V.S. Perun, B.P. Ridenoure, W.G. Read, Z. Shippony, R.A. Stachnik, R.P. Thurstans, and J.W. Waters (joe@camel.jpl.nasa.gov), Mail Stop 183-701, Jet Propulsion Laboratory, California Institute of Technology, Pasadena, CA 91109.

R.L. deZafra and D.T. Shindell, Physics Department, State University of New York at Stony Brook, Stony Brook, NY 11794.

(Received November 9, 1994; revised October 8, 1995; accepted October 8, 1995.)